613

707808

ERDA

Progress Report

Radioisotope Studies Utilizing a Low Level Whole Body Counter and Clinical Applications of Activation Analysis.

July 31, 1977

Prinicpal Investigator

A. B. Brill, M.D., Ph.D.

Vanderbilt University
Medical Center
Nashville, TN 37232

TABLE OF CONTENTS

1. Dosimetric Properties of a New Liver Scanning Agent

A. Introduction

We have carried out organ distribution studies of a new liver scanning agent on four normal male volunteers. The agent, developed by the Abbott Radiopharmaceutical Laboratories, is a technetium labelled stannous colloid prepared with stannous ethanolates (TcSnC). The potential advantage of this compound over other more commonly used liver imaging agents is its ease of preparation and the stability of the labelled compound.

B. Materials and Methods

Each of the four volunteers were injected with approximately 1mCi of ^{99m}Tc-SnC. Blood samples were taken at 15 minutes, 2, 6, and 24 hours. Whole body counts were made at 15 minutes, 2, 6, and 24 hours and quantitative whole body rectilinear scans were made at 1, 6, and 24 hours. The blood samples were counted in an automated well counter requiring at least 10,000 counts above background per sample. The results were expressed as a fraction of the injected dose per ml of whole blood after correction for physical decay of the Tc-99m. The whole body counts were expressed as a fraction of the initial measurement--(15 minute measurement). The quantitative whole body scans were used to estimate the fraction of the injected material in the liver, spleen, and bone marrow. Regions of interests (ROI) were selected from digital whole-body images displayed in a 64 x 64 image format. The integrated counts in the ROI's from the dual opposed detector scanner images were used to determine tha geometric mean (GM) counts of a ROI. (The geometric mean is the square root of the product of the counts from the top and bottom detectors.) The GM counts of each ROI were then expressed as a fraction of the total-body GM counts. Those fractions were then expressed as a fraction of the administered dose by way of the whole body count measurements. The counts from each ROI were corrected for background before computing the GM.

The data from the four studies were grouped together to form a single data set. The data from the blood, total-body, liver and spleen ROI's were used to obtain the equations for the biological retention of the compound. The equations were expressed in the form of a sum of exponentials.

C. Absorbed Radiation Dose Estimates

1. Biological Data

The dose estimates were based upon total body, blood and organ content measurements derived from blood sampling and external measurements of the radioactivity. The results of these measurements are summarized in Table 1. The results are presented as the mean of the measurements from the four studies.

The blood pool activity was derived using blood volume estimates based upon body weight for normal adult males. The upper limit of the marrow activity was determined by assuming that the marrow contained all activity not residing in the liver and spleen or in circulation. Equations 1-5 are the resulting retention functions.

Table 1

(% of administered activity)

Time (hours)	Blood (%/ml)	Blood* (%)	Total Body (%)	Liver & Spleen (%)	Liver (%)	Spleen (%)	Bone** Marrow
0.25	0.00164 ± 0.00008	---	100.0	---	---	---	---
1.00	---	7.7 ± 2.0	100.0 ± 1.0	79.1 ± 3.2	52.4 ± 4.7	26.4 ± 3.8	13.2 ± 4.0
2.00	0.00107 ± 0.00018	---	---	---	---	---	---
3.00	---	---	97.9 ± 3.0	---	---	---	---
6.00	0.00074 ± 0.00034	3.9 ± 1.7	96.8 ± 2.0	79.0 ± 2.4	52.5 ± 3.6	26.6 ± 2.5	13.9 ± 3.5
24.00	0.00035 ± 0.00010	1.8 ± 0.4	83.9 ± 4.0	70.6 ± 4.0	46.7 ± 1.8	23.8 ± 5.8	11.5 ± 6.5

* Calculated using blood volume estimate based upon body weight for normal adult males.

** Estimated using the following equation: Marrow = total body - blood - liver - spleen.

$$\text{Blood } (t) = 4.2e^{\frac{-0.693t}{20}} + 3.5e^{\frac{-0.693}{1.5}t} \quad (1)$$

$$\text{Total body } (t) = 100e^{\frac{-0.693t}{100}} \quad (2)$$

$$\text{Liver } (t) = 53e^{\frac{-0.693t}{100}} \quad (3)$$

$$\text{Spleen } (t) = 26e^{\frac{-0.693t}{100}} \quad (4)$$

$$\text{Marrow } (t) = 13e^{\frac{-0.693t}{100}} \quad (5)$$

(t in hours, activity in percent of injected)

1034711

2. Nuclear Data

TABLE II

Physical Properties

Radionuclide	^{99m}Tc
Physical half-life	6.03 hours
Decay Constant	0.1149 $hours^{-1}$
Δ (equilibrium dose constant for non-penetrating radiation)	0.0369 g. rad/μCi.hour

Principal Photons

	Ei	ni
Ei, energy	0.0186*	0.077
ni, mean number/dis.	0.1405	0.879

* Weighted mean energy of k-x-rays.

TABLE III

CUMULATIVE ACTIVITY ($\tilde{A}$)

$(\frac{\mu Ci.hours}{\mu Ci})$

ORGAN	$\tilde{A}$
Blood	0.34
Total body	8.70
Liver	4.61
Spleen	2.26
Marrow	1.13

Table IV

Average Does Equivalent per Unit

Accumulated Activity (rad/μCi . day)

Target/Source	Blood	Total Body	Liver	Spleen	R. Marrow
Liver	---	5.21×10^{-5}	1.10×10^{-3}	2.36×10^{-5}	2.21×10^{-5}
Spleen	---	5.30×10^{-5}	2.20×10^{-5}	7.99×10^{-3}	2.21×10^{-5}
R. Marrow	---	6.92×10^{-5}	3.88×10^{-5}	4.11×10^{-5}	7.55×10^{-4}
Testes	---	3.98×10^{-5}	1.50×10^{-6}	1.16×10^{-6}	1.09×10^{-5}
Total Body	---	4.69×10^{-5}	5.38×10^{-5}	5.37×10^{-5}	5.21×10^{-5}
Blood	7.38×10^{-6} *	---	---	---	---

* Nonpenetrating radiation only--(Blood Mass = 5000g)

D. Summary of Dose Estimates

The decay corrected biological retention curves for ^{99m}Tc-SnC are presented in Figure 1. A number of conclusions may be drawn from these data:

1. The TcSnC appears to be stable within the body. Measurements at 1 and 6 hours showed very little difference, suggesting no excretion or redistribution. This would indicate that the timing of the diagnostic imaging procedure is not critical at least within a time period of up to 6 hours after injection.

2. The organ distribution of TcSnC is signigicantly different than the expected distribution of Tc-sulfur colloid (in normal subjects). As reported in the Mird report (J. Nuc. Med. (16), 1975, 0. 108) the liver, spleen and red marrow account for 85, 7 and 5 percent of the administered dose, respectively. This compares with 52, 26, and 13 respectively, for TcSnC. Earlier measurements on Tc Sulfur Colliod in our laboratory, using the same instrumentation as was used for the current study, yielded a range of liver to spleen ratios of 2.7-14.1. This compares to a range of 1.7-2.7 for our current study. The increased spleen activity can also be appreciated from the liver/spleen images shown in Figure 2. In each subject signigicant marrow uptake was seen on the image. This finding is consistent with the calculated marrow uptake of 13% in comparison to 5 percent for Tc sulfur colliod. The different "expected" or "normal" distribution presented by this agent means that diagnostic criteria determined from Tc sulfur colloid images can not be applied when reading images made with TcSnC.

The difference in the organ distribution patterns relative to Tc sulfur colloid is reflected in the dose estimates for the two compounds (summarized in Tables V and VI). Liver, gonadal and total body doses are decreased while spleen and red marrow doses are increased. The most signigicant differences being approximately a factor of 3 for the spleen and a factor of 2 for the red marrow.

Table V

Average dose $\bar{D}$ (rad/mCi administered)

(Normal adult males)

TcSnC

Target/Source	Blood**	Total Body*	Liver	Spleen	Red Marrow	Total
Liver	---	0.018	0.211	0.002	0.001	0.214
Spleen	---	0.019	0.004	0.752	0.001	0.757
R. Marrow	---	0.025	0.007	0.004	0.036	0.047
Testes	---	0.014	0.0003	0.0001	0.0005	0.0009
Total Body	---	0.017	0.010	0.005	0.0024	0.0174
Blood	0.0001	---	---	---	---	0.0001

* Calculated assuming normal blood volume

** Nonpenetrating only

Table VI

Comparison of Average Dose (rad/mCi administered)

(Normals)

	TcSnC	Tc Sulfur Colloid*
Liver	0.214	0.34
Spleen	0.757	0.21
R. Marrow	0.047	0.027
Testes	0.0009	0.0011
Total Body	0.0174	0.019

* Mird report J. Nuc. Med. (16) 1975, p. 108

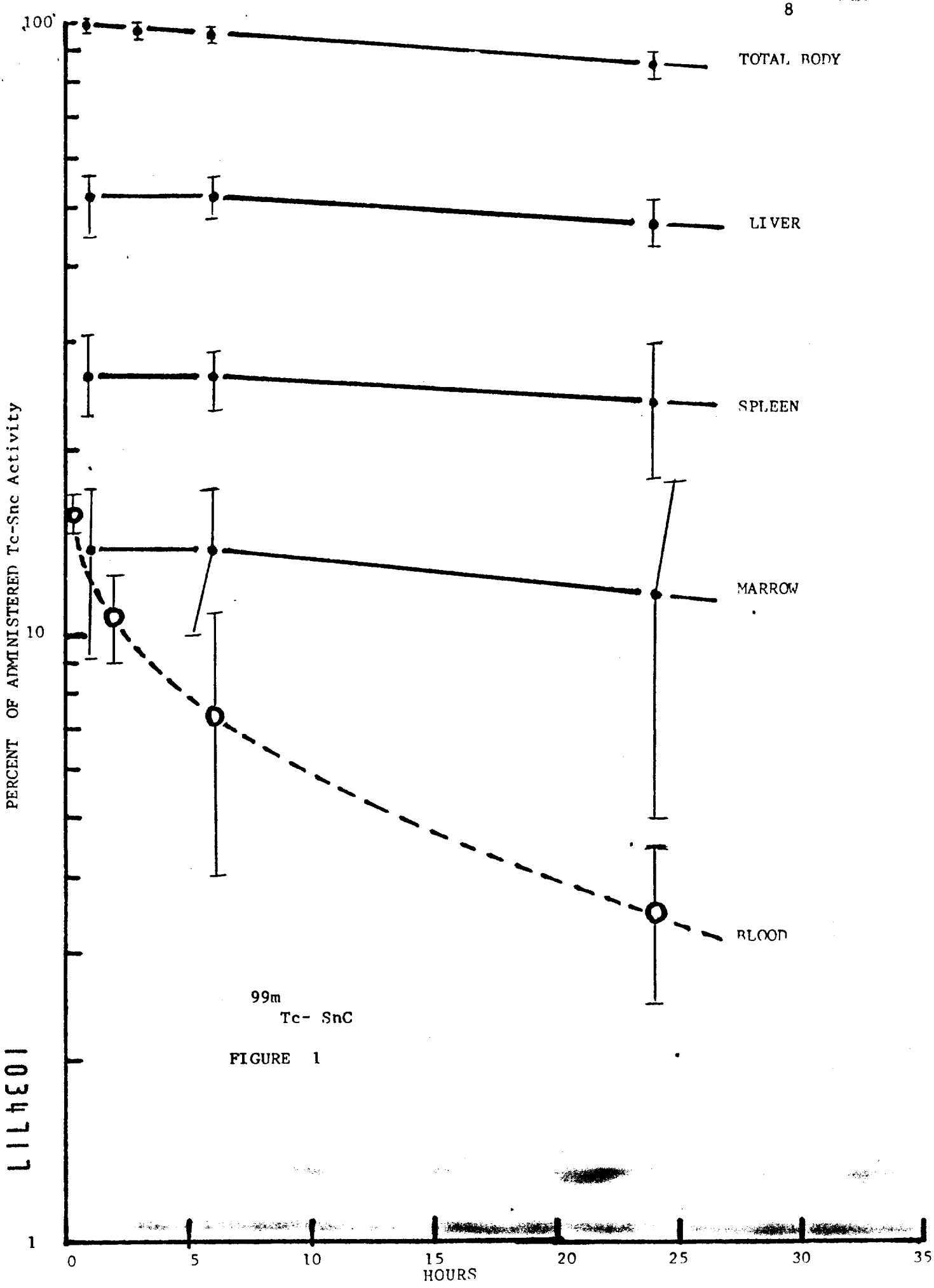

99m
Tc- SnC

FIGURE 1

99m
Tc SnC Liver Agent

ANT. POST.

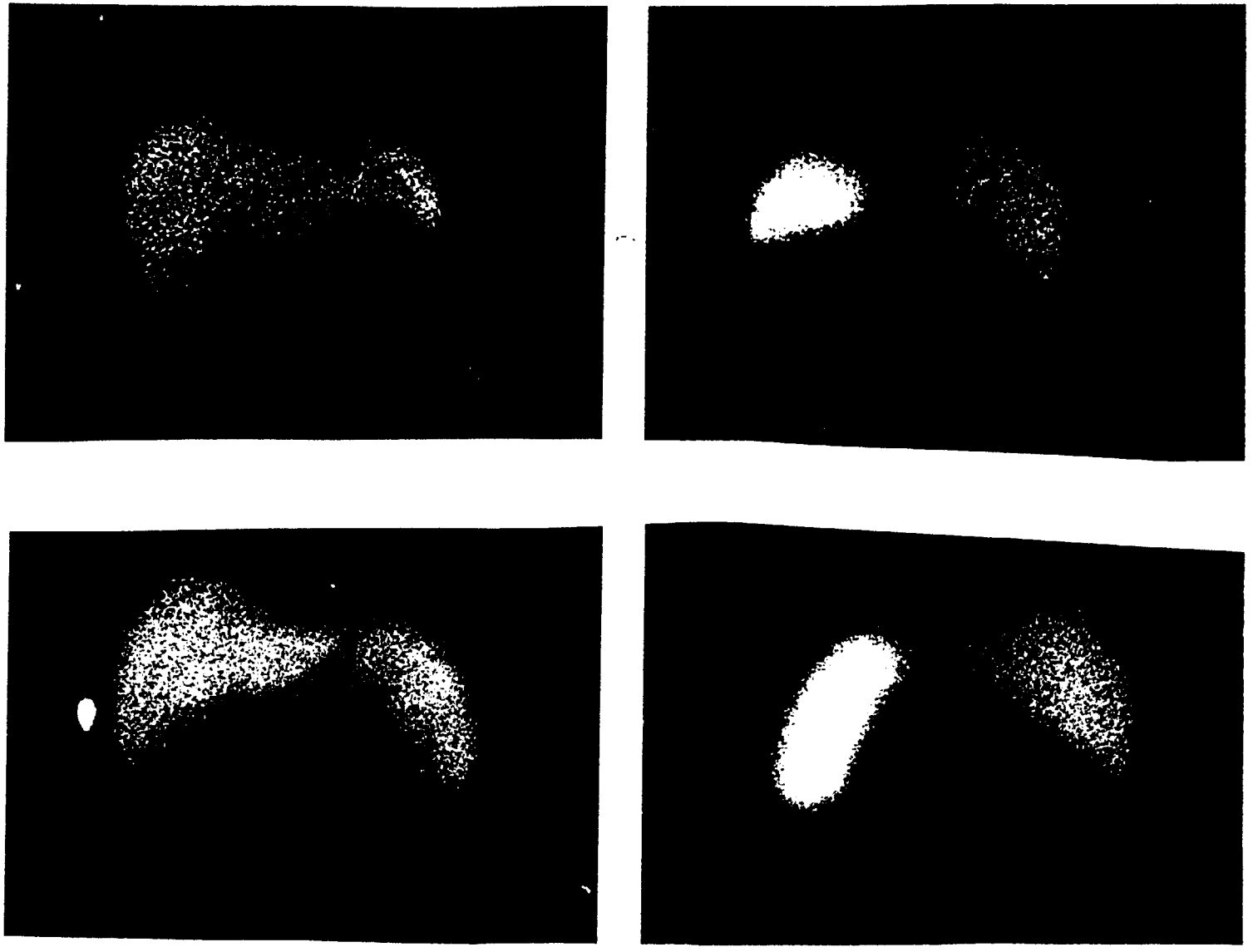

1034718

FIGURE 2

2. Comparative Dosimetry of Iodocholesterol Adrenal Scanning Agents

The development of I-131-19 iodocholesterol (19IC) as an adrenal scanning agent by Beierwaltes and colleagues at the University of Michigan provided an important tool for diagnosing and localizing adrenal disease. Unfortunately, photon densities are low and significant radiation doses were associated with the procedure.

In 1974, we carried out studies in 24 abnormals (adrenal disease) and 6 normals to measure the time-retention kinetics and associated radiation dose from 19IC. The results of this work were included in an earlier report. Since that time it has become apparent that the material obtained from the Pheonix Laboratories was contaminated with varying amounts of a second iodocholestrol compound, namely the ^{131}I-6-iodo methyl norcholestorol (6NC). These two compounds have now been separated, and Searle is planning to distribute the 19IC, while Phoenix Lab is preparing to distribute 6NC for adrenal visualization studies.

We have carried out studies on approximately 25 patients with various adrenal disorders using the Searle 19IC agent with approximately 10 of these patients having repeated studies after being placed on medical therapy. The results of the organ distribution measurements and the related radiation dose estimates are presented in Table 1-9 and Figures 1-7. Representative examples of the adrenal images are shown in Figure 8.

Recently we have acquired shipments of the 6NC compound and have made measurements on 4 patients. All four patients had been studied earlier with the Searle 19IC agent. The improvement of the diagnostic quality of the adrenal images (Figure 8) has been remarkable. However, the biological retention of the new agent relative to the 19IC agent appears to be significantly greater. (A comparison of the 19IC with the 6NC for the total body, liver, left upper quadrent, G.I., thyroid, and rectum and bladder regions can be found in Figures 1-7.)

Since the preliminary results with the 6NC compound look so promising from the clinical standpoint, it appears that this compound will become the favored adrenal imaging agent. In view of this with the added information from our preliminary studies that indicate a substantially increased radiation dose per unit of administered activity, we feel that it is essential to obtain a detailed knowledge of the organ distribution and metabolic fate of this new pharmaceutical. In cooperation with Dr. John Hollifield from the Department of Endocrinology, we are preparing to study an additional 20 patients using a revised protocol during the next year. The revised protocol is being implemented to ascertain whether or not diagnostic quality images can be obtained at earlier times than were required for the 19IC agent (7 to 11 days). If possible, we will propose a reduction of the administered activity which will result in a reduction in the radiation absorbed dose.

Radiation absorbed dose estimates have been completed on the 19IC compound. Preliminary dose calculations have also been made for the 6NC compound. It should be pointed out that the 6NC results are preliminary and are based on a limited number of measurements. More data will be forthcoming during the coming year.

The following two sections detail the biological data and develop the comparison of the organ distributions and corresponding dose estimates for the two compounds.

I. ^{131}I-19-Iodocholesterol

Previous does estimates have been made using the model of cholesterol kinetics proposed by Bernard and Hayes. The model (shown below) is a catenary compartmental model which assumes instantaneous uptake of the material in the liver with an unidirectional flow in sequence through the small intestine first and then through the large intestine exiting in the feces. The model assumes no reflux, retention or transfer of activity across the intestine wall.

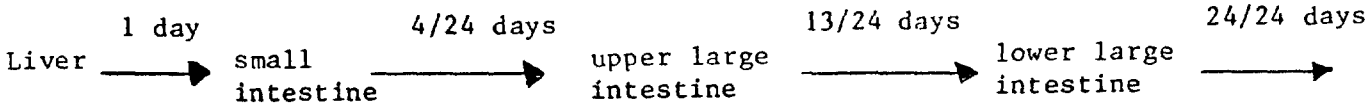

Utilizing the data presented in Figures 1-8, we have generated the data presented in Figure 9 in an effort to substantiate this model. In Figure 9, we have generated the liver and integrated entire G.I. tract activity curves. The curves were generated assuming the liver and right upper quadrant data on day 0 constituted liver activity and that the sum of the left upper quadrant, mid G.I., and the rectum at all other measurements constituted integrated G.I. activity. The resulting curves showed amazingly good agreement with the model prediction. The liver was found to have an uptake of approximately 72% with a monoexponential release of the activity with a half-life of approximately 1 day. The G.I. activity was observed to have a delayed peak occuring at day 1 with a subsequent monoexponential decay of approximately 1.5 days.

The total body retention curve also corroborates the liver measurement by displaying an exponential component with an approximately 2 day half-life and an intercept of approximately 70%. This is interpreted as the fraction of the material that is eliminated via the G.I. tract (72%). The remaining activity (28%) was assumed to be uniformly distributed in the total body and eliminated via the urine with a biological half-life of 1.5 days.

The thyroid data was used to estimate an average uptake of $\sim$ 1%. It was assumed to have an effective half-life equal to the physical half-life.

The adrenal activity was taken to be 0.1%. These data were based upon surgical samples and were assumed to come from a normal sized gland of 16 g. The effective half-live was also taken to be equal to the physical half-life. Having established the consistency of the model for the 19IC agent, the model was used to determine the following cumulative activities for the liver, small and large intestines.

Cumulative Activity

^{131}I-19IC

Organ	$\tilde{A}$ ($\frac{\mu Ci \cdot hours}{\mu Ci\ administered}$)
Total Body	12.7
Liver	22.5
Thyroid	2.8
Adrenals	0.28
Small Intestine	3.81
U. Large Intestine	11.02
L. Large Intestine	18.10

The cumulative activity was then used along with nuclear data shown Table 8 . To generate the continuation of the penetrating and non penetrating components of the absorbed dose. The results of these calculations are shown in table 2 and summarized in Table 3 .

Table 1

I-131-19-Iodocholesterol

(% of Administered Activity)

	Day 0	Day 1	Day 2	Day 3	Day 4	Day 5
Total Body	1.00	1.02 ± .71	.38 ± .06	.19 ± .07	.15 ± .07	---
Liver	.60 ± .05	.33	.08 ± .03	.04 ± .01	.03 ± .01	---
Upper Left Quadrant	.12 ± .03	.12	.06 ± .03	.04	.03 ± .01	---
Mid GI	.03	.05	.04 ± .02	.02 ± .01	.010 ± .006	---
Bladder & Rectum	.06 ± .01	.07	.05 ± .04	.027 ± .002	.02 ± .01	---
Thyroid	.05 ± .04	.03	.02 ± .01	.02 ± .01	.04 ± .02	---
Unaccounted For	.15 ± .06	.08 ± .06	.05 ± .03	.05 ± .03	.02 ± .01	---

	Day 6	Day 7	Day 8	Day 9	Day 10	Day 11
Total Body	.16	.05 ± .02	.049 ± .009	.065	.04 ± .03	.017 ± .007
Liver	.032	.008 ± .004	.005	.008	.010	.003
Upper Left Quadrant	.02	.006 ± .005	.007 ± .004	.027	.002	.002 ± .001
Mid GI	.01	.004 ± .003	.004	.01	.003 ± .001	.002 ± .003
Bladder & Rectum	.01	.005	.005 ± .002	.001	.003	.002 ± .001
Thyroid	.06	.01 ± .01	.010 ± .017	.0006	.04	.006 ± .005
Unaccounted For	.02	.01 ± .01	.016 ± .008	.02	.010 ± .007	.004 ± .002

Table 1 Ctd.

I-131-19-Iodocholesterol

(% of Administered Activity)

Continued

	Day 12	Day 13	Day 14
Total Body	.015 ± .003	---	.008 ± .003
Liver	.003	---	.002
Upper Left Quadrant	.002	---	.001
Mid GI	.002 ± .001	---	.001
Bladder & Rectum	.001	---	.001
Thyroid	.002	---	.002 ± .003
Unaccounted For	.005 ± .002	---	.004

Table 2

19IC

Average Dose ($\bar{D}p$ rads/mCi)

(Penetrating Component)

Target/Source	Total Body	Liver	Small Intestine	ULI	LLI	Total (rads/mCi)
Total Body	0.049	0.107	0.020	0.058	0.096	0.330
Liver	0.059	1.600	0.020	0.060	0.017	1.756
S. I. Wall	0.068	0.102	0.330	0.374	0.046	0.920
ULI Wall	0.071	0.158	0.245	0.896	0.214	1.584
LLI Wall	0.065	0.019	0.073	0.091	2.552	2.800

(Non-penetrating Component)

Organ	$\bar{D}np$
Total Body	0.075
Liver	5.06
S.I.	0.928
U.L.I.	10.90
L.L.I.	23.4
Thyroid	58.2
Adrenal	7.3

Dose Summary ($\bar{D}$ rad/mCi)
(19-IC)

Organ	$\bar{D}p$	$\bar{D}np$	$\bar{D}$ total
Total Body	0.330	0.075	0.405
Liver	1.756	5.06	6.82
S.I. Wall	0.920	0.928	1.848
ULI Wall	1.584	10.90	12.48
LLI Wall	2.800	23.4	26.2
Thyroid	---	58.2	58.2
Adrenal	---	7.3	7.3

II. ^{131}I-6 Iodomethyl Norcholesterol (6NC)

[redacted]

Table 4

6 Nor Methyl

(% of Administered Activity)

	Day 0	Day 2	Day 4	Day 5	Day 7	Day 11
Total Body	1.00	.69 ± .10	.33 ± .01	.35	.22 ± .05	.16 ± .09
Liver	.53 ± .09	.20 ± .03	0.079 ± .002	.06	.05 ± .01	.04 ± .02
Upper Left Quadrant	.23 ± .02	.11 ± .01	.05 ± .01	.08	.05 ± .009	.02 ± .02
Mid GI	.05 ± .03	.06 ± .01	.032 ± .004	.08	.02 ± .01	.02 ± .02
Bladder & Rectum	.08 ± .02	.148 ± .022	.075 ± .002	.060	.05 ± .02	.03 ± .01
Thyroid	.03 ± .01	.023 ± .009	.023 ± .009	.014	.02 ± .02	.008 ± .002
Unaccounted For	.08 ± .04	.11 ± .01	.09 ± .02	.06	.05 ± .01	.028 ± .002

Table 5

Cumulative Activity

6NC

Organ	$\tilde{A}$ $\frac{\mu Ci \cdot hour}{\mu Ci}$
Total Body	10.9
Liver	33.0
Thyroid	2.8
Adrenal	---

Table 6

Dose Summary

($\bar{D}$ rad/mCi)

6NC

Organ	$\bar{D}p$	$\bar{D}np$	$\bar{D}$ total
Total Body	0.121	0.064	0.19
Liver	2.40	7.59	9.99
Thyroid	---	58.2	58.2

Table 7

Dose Comparison

$\bar{D}$ (rad/mCi administered)

Organ	19IC	6NC
Total Body	0.045	0.19
Liver	6.82	9.99
Thyroid	58.2	58.2
S.I.	1.85	---
U.L.I.	12.5	---
L.L.I.	26.2	---

relative to the 19IC agent. As shown in Table 7, the dose to the liver from the 6NC is increased by approximately a factor of 1.6 over the liver dose from 19IC. We anticipate a commercially increased dose to the samll and large intestines.

3. The uptake of the 6NC in the adrenals is much greater than that of the 19IC. Although this leads to larger doses if one continues to use the same level of injected dose--the natural course is to reduce the level of the administered activity.

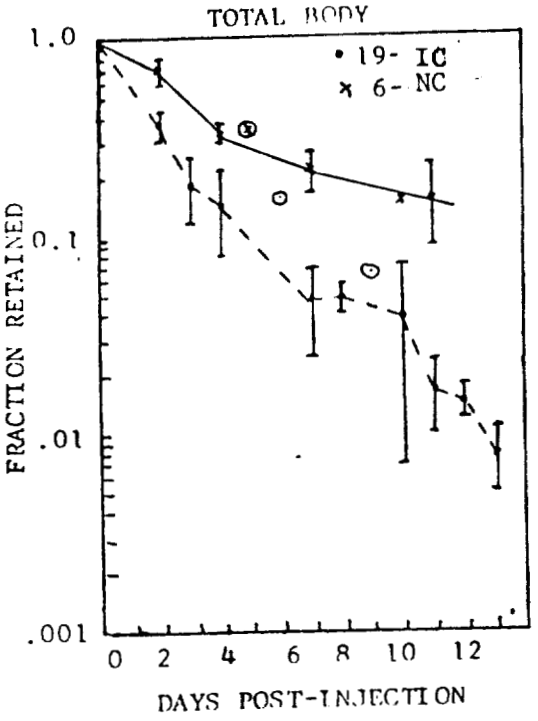

FIGURE 1

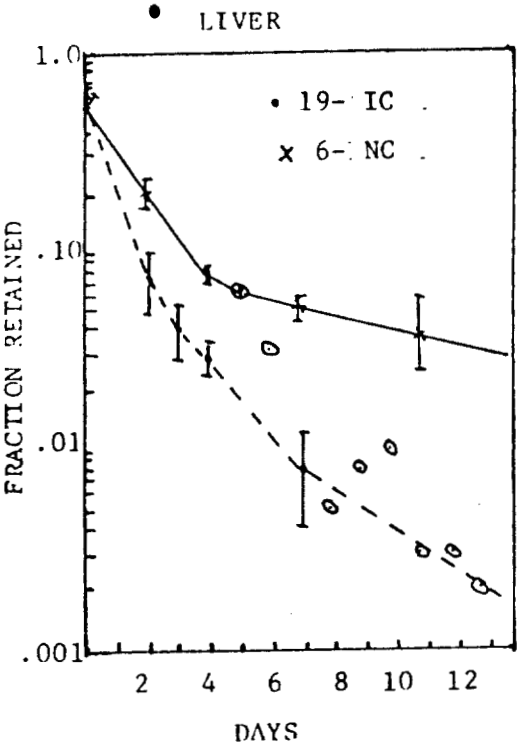

FIGURE 2

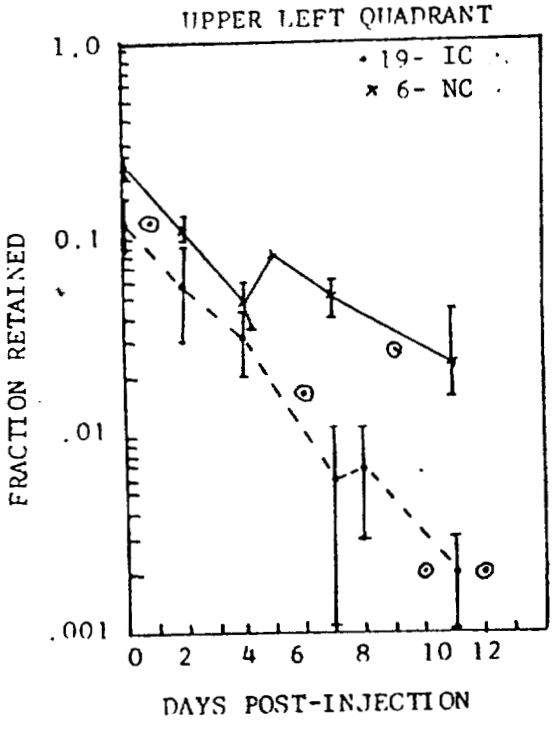

FIGURE 3

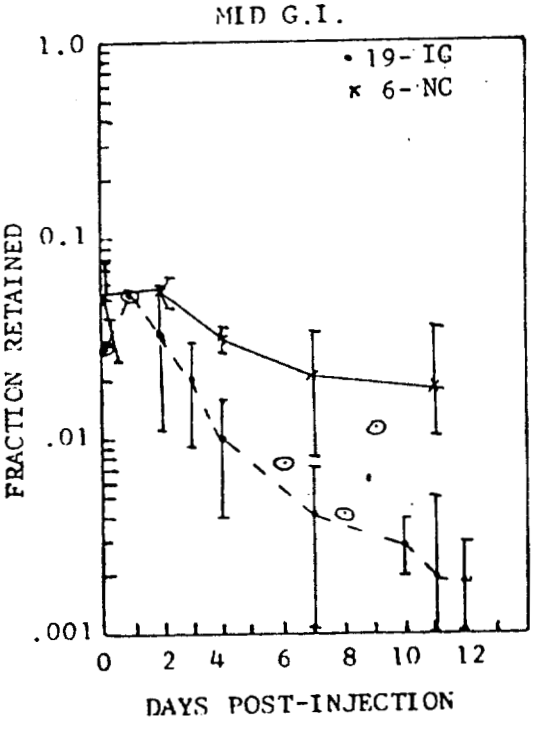

FIGURE 4

1034730

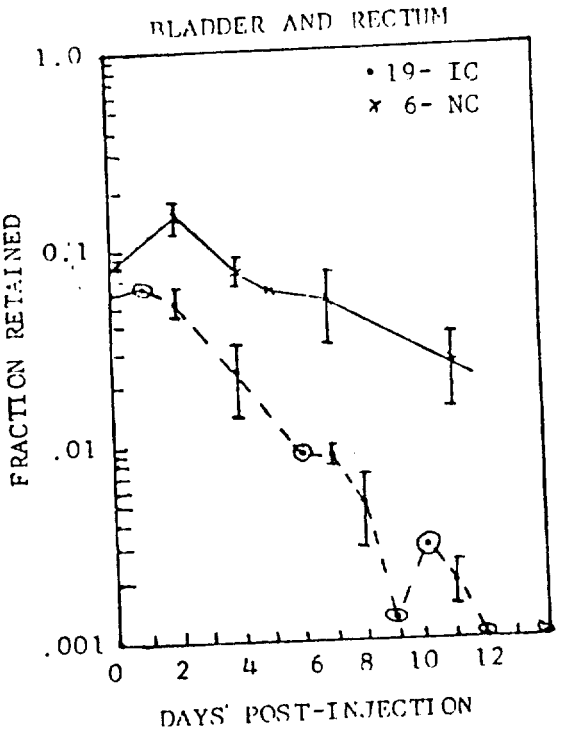

FIGURE 5

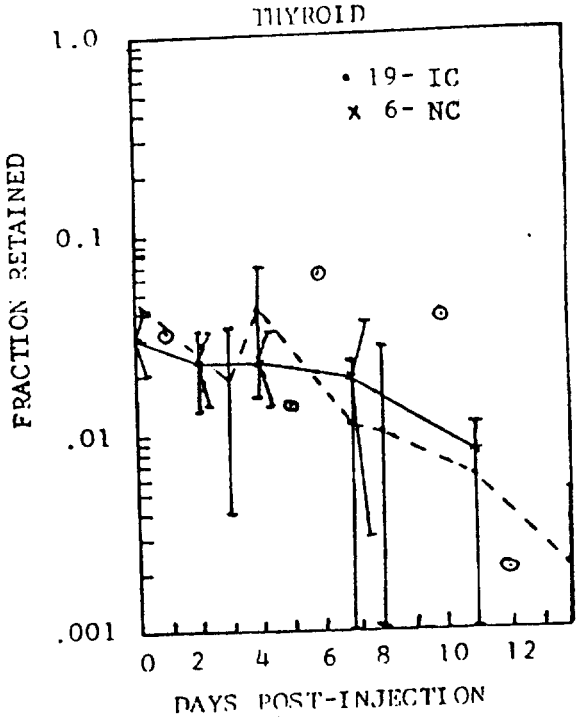

FIGURE 6

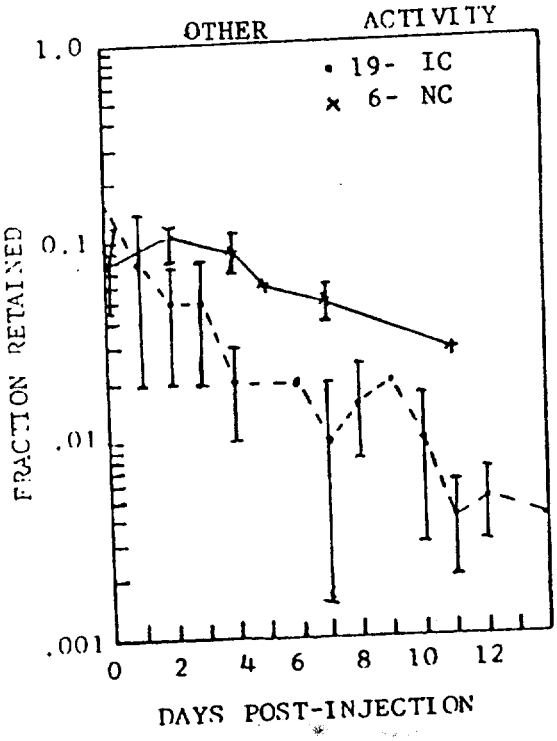

FIGURE 7

DAY 7

19 IC 6 NC

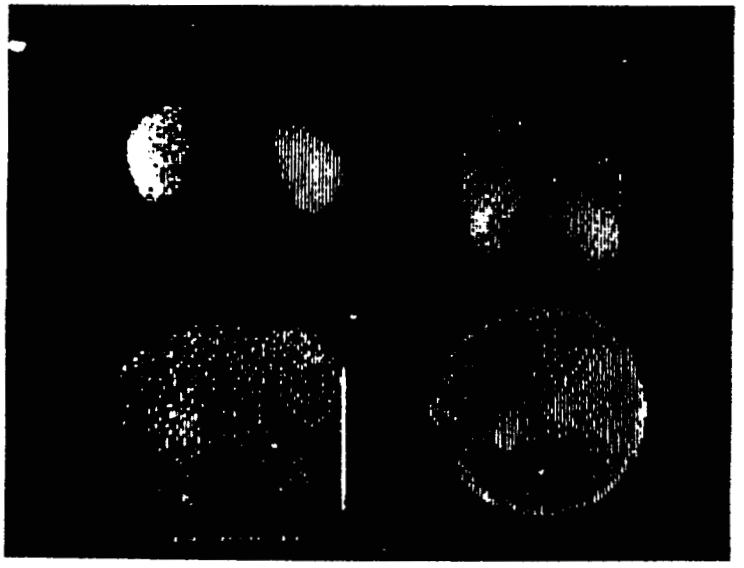

KIDNEY
Tc-DMSA

ADRENAL

DAY 11

19 IC 6 NC

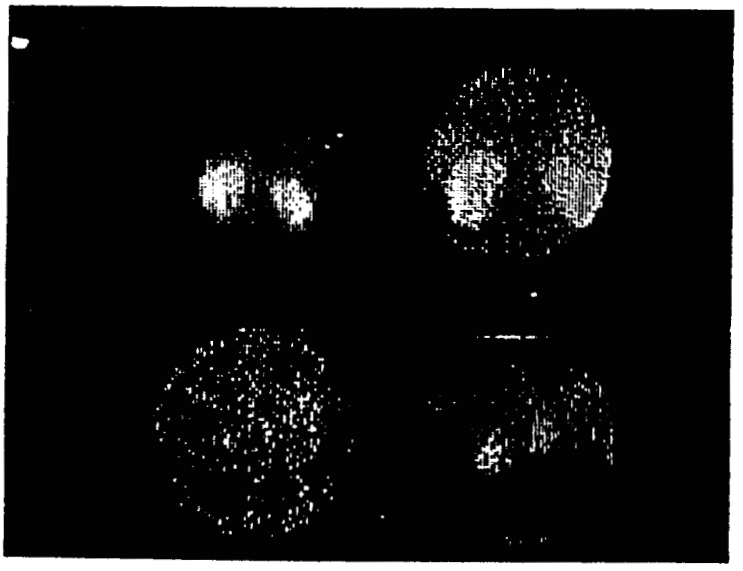

KIDNEY

ADRENAL

FIGURE 8

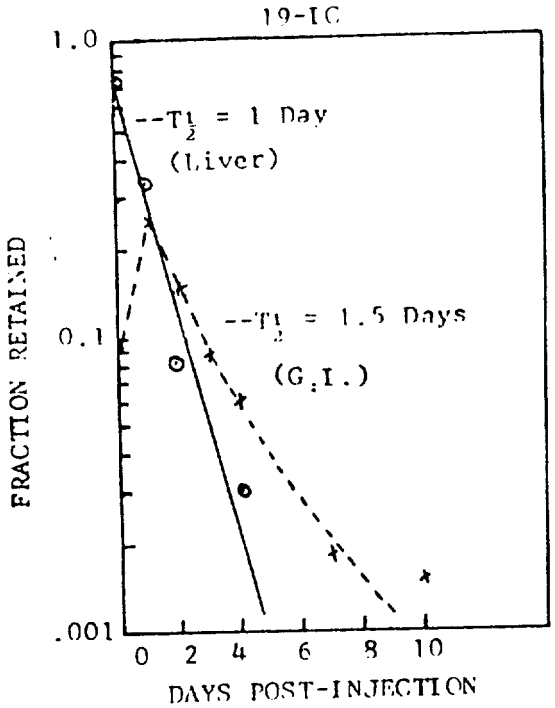

FIGURE 9

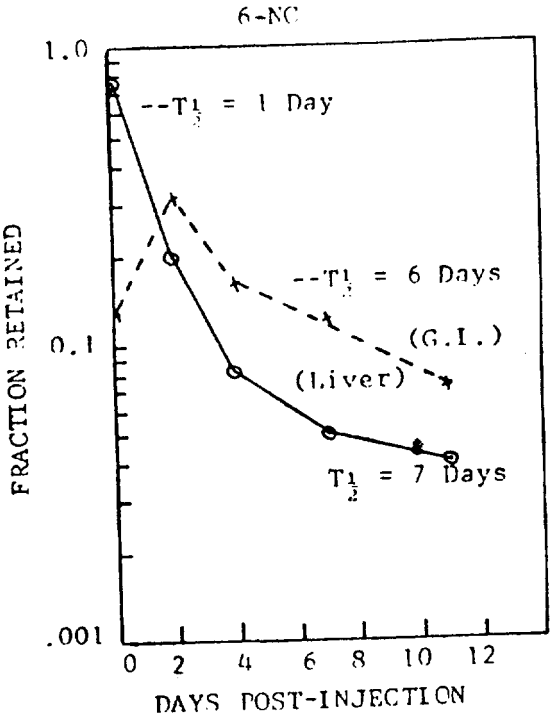

FIGURE 10

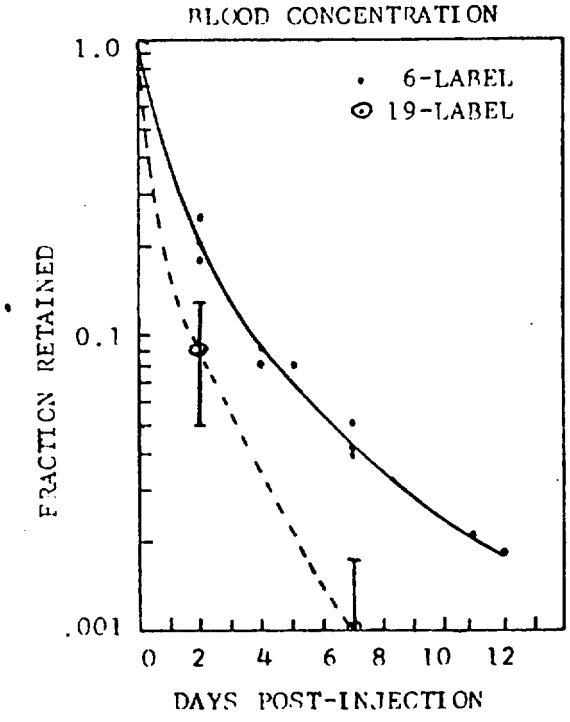

FIGURE 11

Table 8

Nuclear Data (MIRD Pamphlet No. 2)

Radionuclide	^{131}I
Physical half-life	8.05 days
Decay Constant	3.59×10^{-3} hours^{-1}
Δ (equiliberium dose constant for nonpentrating radiation)	0.4135 $\frac{g \cdot rad}{\mu Ci \cdot hour}$

Prinicple Photons

	Ei	Δi
Ei, energy	0.0801	0.0030
	0.1772	0.0005
Δi (equilibruim)	0.2843	0.0288
(dose constant)	0.365	0.6477
	0.5 - 0.72	0.1211
	K X-rays	0.0030

Table 9

Blood Levels

(% of Administered Dose)

Compound	Day 0	Day 2	Day 3	Day 4	Day 7	Day 11
19IC	100	---	9.3 ± 4.2	---	1.0 ± 0.5	0.3 ± 0.1
6NC	100	21.2 ± 3.6	---	8.5 ± 0.7	4.4 ± 0.6	2.0 ± 0.1

3. Renal Dosimetry

In our ongoing interest to assess the radiation dose associated with routine diagnostic procedures, we have become particularly interested in the dosimetric problems associated with inhomogenous radioisotopic distributions. Inhomogenous distributions are frequently encountered in I-131 hipuran renograms of transplanted kidneys. The transplanted kidney is prone to urine flow obstructions resulting in prolonged clearances of the labelled hippuran. In particular the renal pelvis (a relatively small fraction of the entire renal mass) may retain essentially the entire injected activity for an extended period of time. During the past year we have attempted to establish mechanisms and developed computer programs to acquire the data necessary to make realistic dose estimates for the renal pelvis from routine renograms performed on renal transplant patients. Unfortunately for this project during the past year the data collection instrument used for the routine renograms was changed. We orginally used an Intertechnique cinescintigraphy system and have now switched to the PDP-11/Gama-11 System. This switch has required the development of new programs to collect the data and develop the kidney and separate pelvis time--activity curves. The system has just recently become operational and consequently a limited number of studies have been performed. We are continuing this work and hope to acquire data, on approximately 100 cases exhibiting varying levels of pelvic accumulation within the next 3 months.

Table 1 shows some of our preliminary results. The table presents three patients with renal pelvic accumulation of the I-131-hipuran ranging from moderate to strong. For the case where little pelvic accumulation occured, the dose to the pelvic region is only one percent greater than the average dose. For the second case, the cumulated concentration in the renal pelvis is 32% greater than the average total kidney concentration, and 47% greater than the concentration in the renal parenchyma. Thus the dose due to non-penetrating radiation from I-131 is 47% higher in the renal pelvis than the rest of the kidney. For the third case, the dose due to non-penetrating radiation from I-131 is seen to be 71% higher in the renal pelvis than in the kidney as a whole, and 239% higher than in the parendryena.

These preliminary data indicate significant doses may result from pelvic accumulation. We feel a continued effort in this pursuit is warrented. As part of this work we will attempt to make more accurate estimates of the volume and mass of the pelvis in order to improve our dose estimates. In addition to the pelvis self-dose, we will also assess the gonadol dose resulting from the nearby pelvis activity.

Table 1

	Total Kidney	Renal Parenchyma	Renal Pelvis Accumulation
Case I			
Cumulated Concentration (Arbitrary Units)	51.8	51.4	0.4
Percent Accumulation	0.8%	0.8%	---
Case II			
Cumulated Concentration	67.9	46.2	21.9
Percent Accumulation	32.3%	47.4%	---
Case III			
Cumulated Concentration	38.9	11.5	27.5
Percent Accumulation	70.7%	239%	---

4. Iron-59 Citrate Dosimetry in Abnormal Human Subjects

During the past year, we have continued our work to make quantitative measurements of the absolute organ distribution of intravenously administered Fe-59 citrate in abnormal subjects. In cooperation with Dr. Sanford Krantz of the Department of Hematology, we are carrying out detailed studies on a selected group of patients with suspected and proved red-cell aplasia. Our work has allowed us to observe how the kinetics of the radioiron and the resulting organ distributions may vary greatly from patient to patient depending upon the stage of the disease. The kinetic data we have collected and are using to make dosimetric estimates are also proving useful to Dr. Krantz as an aid to establishing the stage of the disease.

A draft of a paper describing the results of our work on a group of patients who were in remission of the disease has been included as an appendix to our current report. The paper is entitled "Studies on Red Cell Aplasia: Ferro-kinetics During Remission of the Disease". In this paper we have attempted to compute the marrow retention curve of the radioiron in six (6) patients who are in remission of the disease. Dosimetrically, we have determined that the red marrow is the critical organ for patients in full remission while the liver and spleen are the critical organs at other stages of the disease. During remission we have observed great expansions of the active red marrow sites to the knees, ankles, elbows and the long bones of the arms and legs. We have also observed that the expanded marrow sties may also be accompanied by a prolonged transit time for the radioiron resulting in an increased radiation dose to the marrow. We have attempted to estimate the total marrow radioiron retention curve for each of the patients in this group. The results of these measurements are seen in Figure 1-3. These curves are also used to estimate the marrow dose from radioiron within the marrow.

Time-activity curves were generated for the pelvic marrow at approximately one day intervals for an average period of 10 days. Images of the total-body distribution of the radioiron were also made on a daily basis. The time-activity curves for the total marrow were estimated from the direct measurements of the pelvic marrow space. The pelvic marrow transit curve at 24 hours was taken to be equal to the total-body radioiron content minus the liver and spleen content. Two assumptions were that there was no significant circulating level of radioiron at 24 hours and that the liver and spleen constituted the entire storage pool exclusive of marrow. Based upon time-activity curves generated in this manner marrow transit-times were determined. The transit-time was defined as the time interval between the 50% levels of the maximum radioiron uptake in the marrow that occurred during the uptake and release phases. In a manner similar to that described by Finch the plasma clearance and red cell utilization curves were also used to estimate the total marrow activity curves. In this method one assumes the marrow uptake of the radioiron to be proportional to the inverse of the plasma clearance and the marrow release of the radioiron to be proportional to the inverse of the red cell incorporation curve. The curve is then normalized to the maximum activity incorporated into the circulating red cells. An assumption of this method is that the maximum circulating red cell activity is equal to the maximum uptake in the erythropoietically active marrow pool.

The patients in our current study group were classified into three groups with respect to their marrow transit curves. We have observed that the transit curves frequently exhibit two distinct transfer components. We have chosen to describe these two components as (1) erythropoietic (rapid, T-1/2 approximately 3 days) and (2) storage (T-1/2 approximately ∞).

In the normal the second (storage) component is extremely small while in some abnormals the reverse is true. It is the presence and magnitude of the storage components that is the prime contributor to the dose. As shown in Table 1 the three classes have been defined as follows:

A. No significant storage component
B. No significant erythropoietic component
C. Both components present

We have investigated the variation in the radiation dose to the marrow between these three groups. The results of these calculations are shown in Table 2. As seen in the table the marrow dose may be as much as a factor of 19 higher in those patients with significant marrow storage of the radioiron. We hope to be able to extend these measurements and calculations to a larger patient population.

The MIRD Committee in the United States has created a task group to gather dosimetric information from the medical uses of Fe-59 citrate. Dr. Price is a member of this task group and we are working in cooperation with Dr. Pollycove at the Donner Laboratory of the University of California and Dr. Johnston at the University of North Carolina to create a single data base. Vanderbilt's SAAM-25 iron kinetics model has been chosen to be used for the calculation of the cumulative organ activity (A) for the compiled normal and abnormal studies. The results of these measurements and calculations will be published by MIRD. A draft of this document is included as an appendix to our current report.

During the coming year, we propose to continue our relationship with Dr. Krantz and staff of the Division of Hematology and will study approximately 10 more patients in an effort to categorize the dosimetry and kinetics of different disease states.

Dose estimates to date have been made assuming a standard man model. For many of these disease states, the liver and spleen may be enlarged in addition to an expanded or diminished red marrow volume. The effects of these volume differences could be significant and will be investigated. Liver and spleen volume estimates will be made using ultrasonic scans, or with CAT body scans whenever possible. Estimates of the regional marrow volume will be made using the projected area from the Fe-59 scans.

It is known that the marrow spaces in some abnormal states contain a significant amount of the iron storage component. To resolve the functioning marrow components from the storage components using external marrow measurements, we propose to use simultaneous scans of In-111 transferrin and Fe-59. The assumption is that the In-transferrin communicates only with the ferritin hemosiderin (storage) pools and not with the hemoglobin (erythropoietic) pool, and thus, we can use the In-111 distribution to measure the storage pools of the marrow sites for Fe-59. The dosimetric implications of the separation are significant since the kinetics of the two components are so different. Fe-59 labelled to hemosiderin but residing in the marrow space would have an essentially infinite biological half life, whereas Fe-59 labelled hemoglobin leaves the marrow in a matter of a few days. We have proposed to study 10 new subjects this year and will carry out the simultaneous In/Fe study whenever possible.

Table 1

Cumulative Activity

$\tilde{A}$ ($\frac{\text{uCi days}}{\text{uCi adm.}}$)

	Patient Group	$\tilde{A}$
A	Patients with no significant storage component	2.40 - 3.66
B	Patients with no significant erythropoietic component	19.4
C	Patients with both storage and erythropoietic function	40.0

Table 2

Average Radiation Dose to the Red Marrow

$\bar{D}$ (rad/uci adm.)

Group	$\bar{D}$np (nonpenetrating)	$\bar{D}$p (penetrating)	$\bar{D}$ (total)
A	0.008 - 0.012	0.003 - 0.005	0.011 - 0.017
B	0.066	0.027	0.093
C	0.136	0.055	0.191

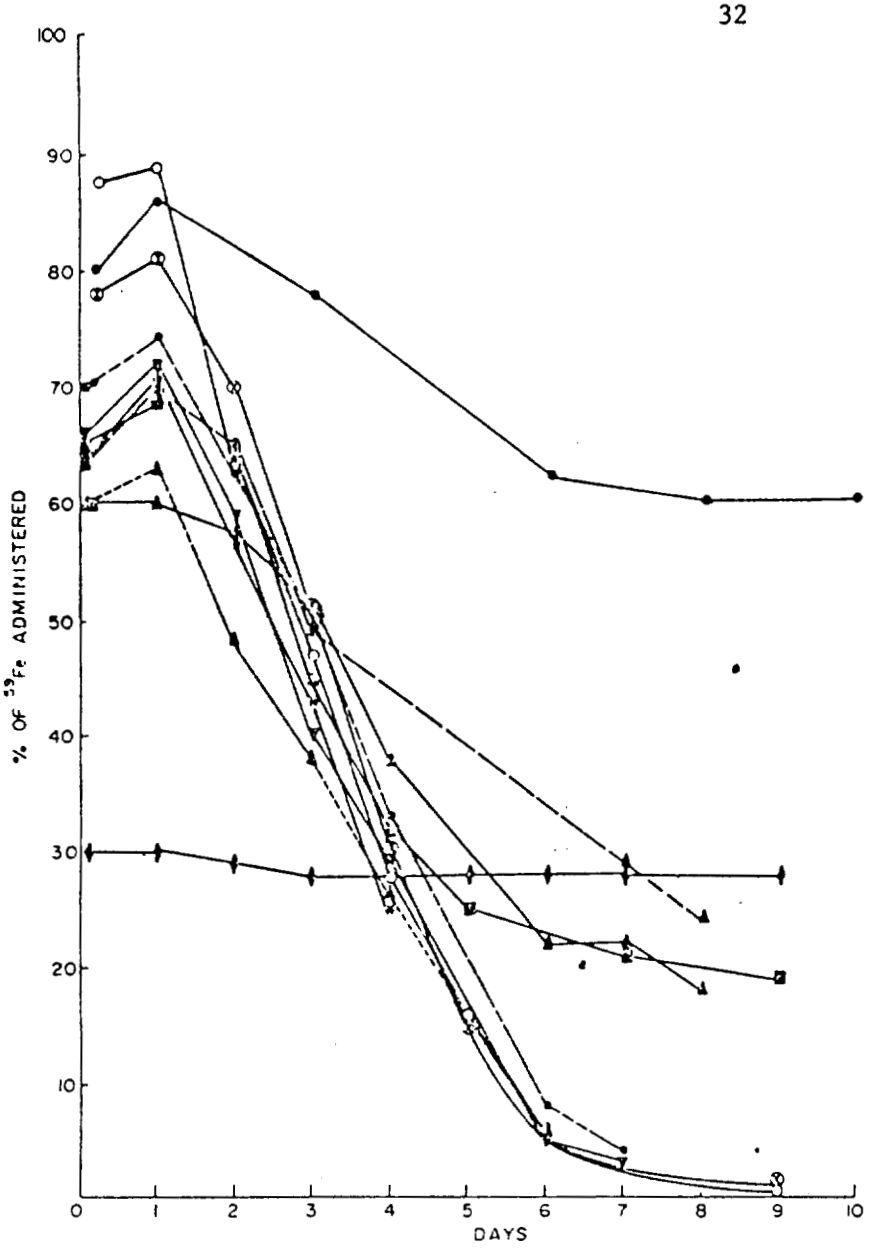

Figure 1. Marrow radioiron transit time curves. Normal volunteers o - o and o—o. Patient number 6 with PRCA ◊-- ◊. Patients with PRCA in remission: number 1, Oct., 74 Δ--Δ, June, 75 Δ---Δ, and Nov., 76 Δ—Δ, number 2, Nov., 73 o—o and Aug., 76 o---o; number 3, □----□; number 4, ▽—▽; number 5, *——*.

PRCA = pure red cell aplasia

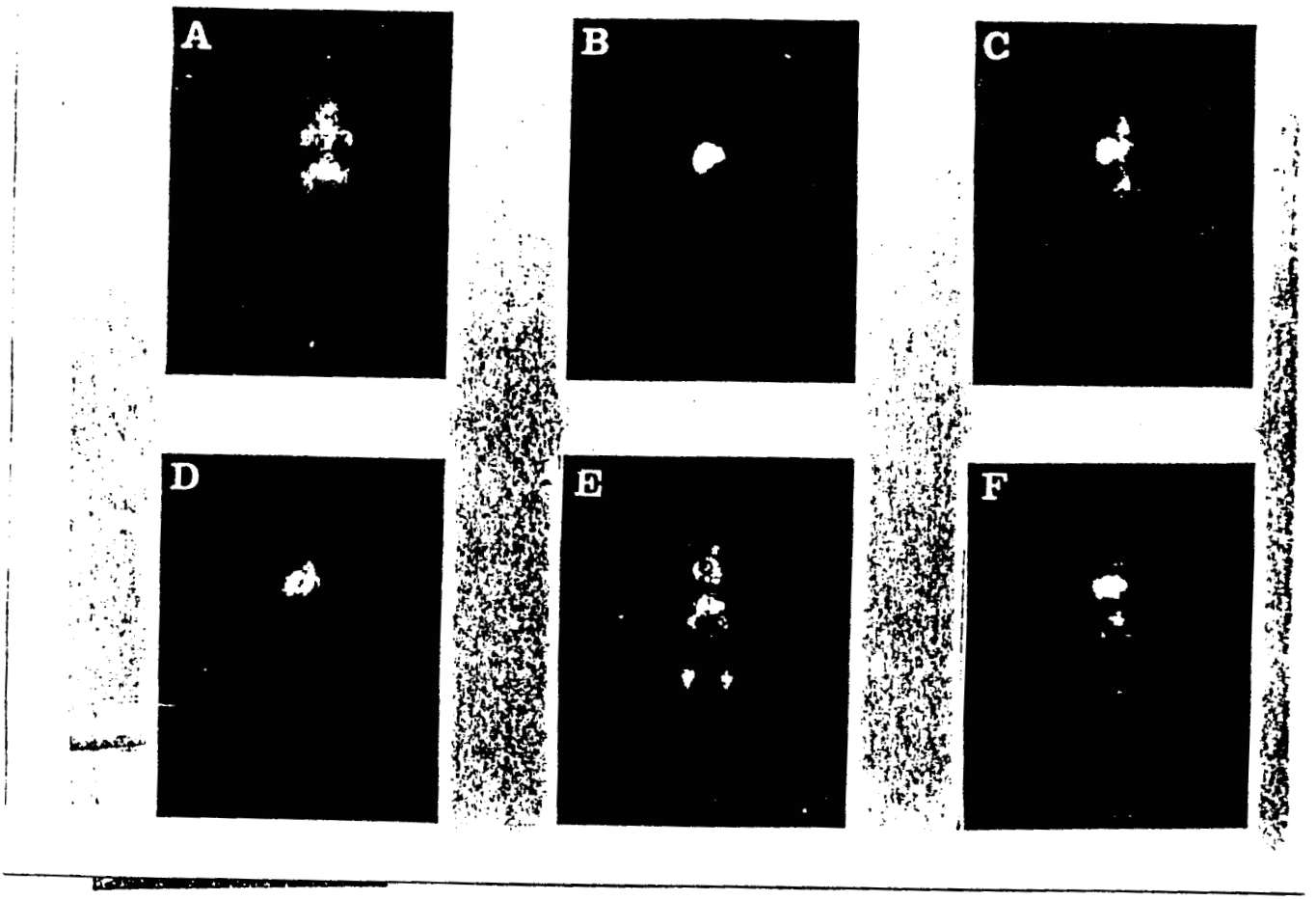

Figure 3. Surface organ scanning (A) Normal volunteer. (B) Patient number 6 with PRCA. (C,D,E,F) Patients with PRCA in remission showing (C) normal marrow distribution of ^{59}Fe in patient number 3, (D) moderate extension of bone marrow into lower extremities in patient number 5, (E) marked extension of bone marrow in patient number 2 in first study after remission, and (F) reduction of marrow extension in patient number 2 three years later.

PRCA - pure red cell aplasia

5. Evaluation of the Standard Man Model for Dosimetry Calculations--Comparison with Laboratory Measurements

One of our staff (Dr. J. Jones) has accepted a position on Scientific Committee No. 55 of the National Council for Radiation Protection and Measurements. This committee, chaired by Dr. James Robertson of the Mayo Clinic, is charged with making recommendations for the experimental verification of internal dosimetry calculations and is scheduled to meet to review a first draft of its report in September, 1977 (our contribution to this draft is included in the Appendix).

We have also completed an evaluation of model calculations with humans, which is reported in a Ph.D. thesis (Dr. Jones) and in the proceedings of the Radiopharmaceutical Dosimetry Symposium held in Oak Ridge in April 1976. The approach used was to expose LiF TLD's on the skin of liver scan patients (Tc-99m sulfur colloid) anterior to and centered over the liver. The measured TLD dose was compared to that computed for the standard man model, with generally acceptable ($\sim$ 30%) agreement between measured dose and calculated dose. However, the model calculations were of dose per emitted photon, so a scheme was developed to compute organ activity from external scanning measurements. This scheme and its derivation are also outlined in the Appendix.

A major question concerning the applicability of model dose calculations to humans is whether or not the combined effects of attenuation and geometry in humans are adequately represented by the model, especially since humans vary in size, shape, and medical condition. If photon attenuation is small enough, these geometry differences will have minimal effect. Conversely, if there are no geometry differences, photon attenuation will have no effect. Conversely, if there are no geometry differences. photon attenuation will have no effect. However, it is certain that in at least some cases, there will be differences, and it is important to evaluate the effects. These attenuation/geometry effects are present for both the radiation dose measurements and the organ activity measurements, but with an important distinction. The dose measurement device is uncollimated and allowed to respond to any photon energy (primary photons incident from various directions and Compton scattered photons). Under these conditions, it is extremely difficult to express the effects of attenuation/geometry on the dose. Organ activity measurements are made with collimated detectors and use pulse height discrimination, in an effort to assure that only primary photons incident from a specific direction are counted. With these conditions, it is possible to express the effects of attenuation/geometry on the activity estimate, which is what our scheme does.

Equations (10) through (13) of this scheme (see Appendix) are the primary relationships of interest. The effects of attenuation are contained in the parameter μ, while the effects of geometry are contained in linear combinations of body thickness dj, source thickness tj, and source depth Zlj. So given a set of dj, tj, and Zlj (geometry) and a value of μ (attenuation), one can express the effects of these parameters on the activity estimate, and compare the result to a similar set of parameters representing the geometry of the standard man model.

We have developed the hardware and software which allows one to trace an arbitrary shape on a graphics tablet and send the coordinates of this shape to a PDP-9 computer for analysis. This can be used on a suitable cross-sectional image (a computed tomography scan or ultrasonic scan) to send coordinates of body and organ outlines to the computer. We have also written programs which use these coordinates to evaluate (12) and (13) for various values of μ (corresponding to photon energies from 20KeV to 1MeV) and present the results

on a line printer. The programs have been debugged using clinical ultrasonic scans, and we are now in the process of creating files of standard man model data for various transverse sections, using the information in MIRD Pamphlet No. 5. Because several physicians in our department are interested in organ volume measurement from CT scan images, the programs have been written to do the volume calculation for their use, as well as the evaluation of these activity equations for our use.

6. Dosimetry of Photon Attenuation Measurement Systems

a. Bone Mineral Measurement Techniques

We have been involved in the development of techniques to measure bone mineral content in the arm and lumbar spine in our laboratory and the procedures that we have developed are now routine clinical procedures in our nuclear medicine clinic. These techniques involve the passage of a pencil thin beam of radiation from an external source through the part of the body under study and the measurement of the attenuation of the beam by an opposed detector as a function of position as the system scans in a rectilinear raster. Since these measurements are made at multiple times in following the course of diseases and evaluating the effectiveness of therapy, the radiation dose from such measurements are of importance.

We have made dose measurements for arm and spine scans using lithium fluoride thermoluminescent dosimeters (TLDs). For arm measurements 12 TLDs were placed on an arm phantom (6 on the top and 6 on the bottom) as shown in figure 1. The phantom consisted of a plexiglass block with three chambers containing a K_2HPO_4 solution to simulate the bone mineral content of the arm. The three chambers were approximately the size of an adult male radius, an adult female radius, and an adult finger. A routine scan was then performed on the phantom using a 2 Ci source of Gd-153. This source emits 40 and 100 keV photons of approximately equal intensity and permits the elimination of the soft tissue component in the bone mineral determinations by the two photon technique. The TLDs were then read out by heating them in an oven and measuring the light given off (which is proportional to the radiation dose received) using a photomultiplier tube. The TLDs were then annealed in order to assure that their sensitivity did not change and they were then exposed to a Cs-137 source of known intensity. They were again read out and a factor was determined relating the known dose rate from the Cs-137 exposure to the light intensity measured by the photomultiplier tube. The dose rate for an arm scan was determined to be less than 40 mrad with the 2 Ci Gd-153 source.

A similar technique was used to measure the dose rate for the spine scans. TLDs were taped along the top and bottom of a tank containing 14.1 cm of water and four excised vertabrae to simulate the spine and soft tissue as shown in figure 2. A scan was performed and the dose rate was determined as before. The dose rate for the 2 Ci Gd-153 source was less than 65 mrad at all points. The individual TLD measurements are summarized in Table I. The radiation dose from these studies is considered to be low enough to permit repeated studies without undue hazard to the subject.

b. Computerized Azial Tomography Systems

The advent of computerized axial tomography systems using high intensity transmission sources has produced concern over the radiation dose associated with such procedures. We have made measurements of typical radiation doses obtained from computerized axial tomographic scans of the head with an EMI head unit. These were measurements of doses received by both patients and the personnel taking part in the administration of the test.

The measurements we made were made by using pre-calibrated TLD's. All measurements were made with either a patient or water filled phantom in place in the water bag of the EMI scanner. The TLD's were placed on the skin of the patient or on the surface of the phantom.

The first measurement we made was a determination of the dose distribution perpendicular to a single scan slice. We found that the exposure fell to less than 400 mrad within .5 cm from the outer edge of the scan slice. By placing a strip of dosimeters vertically down the patient's head during a clinical study (consisting of 5-6½ minute scans) we found that the eyes received a total exposure of 500 millirad. The exposure at the top of the head reached 2.5 rad.

Because the x-ray tube does not travel completely around the head during a scan, we made a measurement of the angular distribution of exposure. This showed a distinct asymmetry in the exposure distribution. The exposure ranges from a maximum of 2.75 on the right side of the patient's head to .75 in the left side of the head.

Often it is necessary for someone to hold a patient's head during a scan in order to help reduce the motion artefacts. We monitored the exposure to this persons hand by means of a ring badge. Depending on the level of the scan, this exposure ranges from 3 mrad to a high of 100 mrad per scan slice. The maximum total exposure received by one person during the course of the measurements was a 200 mrad.

Based on these measurements we recommended that personnel who routinely assist in this manner should make a practice of wearing protective gloves.

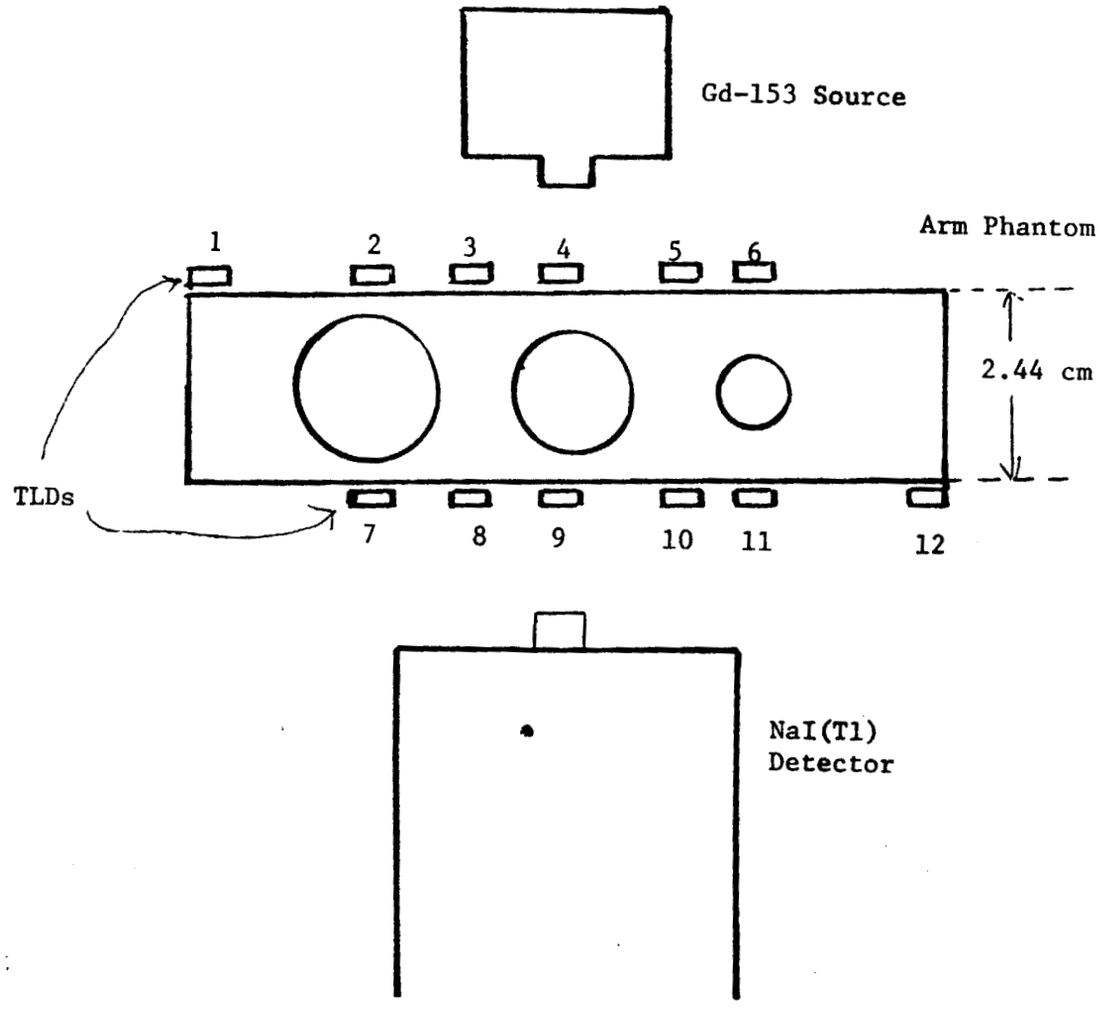

Figure 1 Diagram of transmission scan apparatue for determination of dose to the arm when measuring bone mineral content of the radius and ulna.

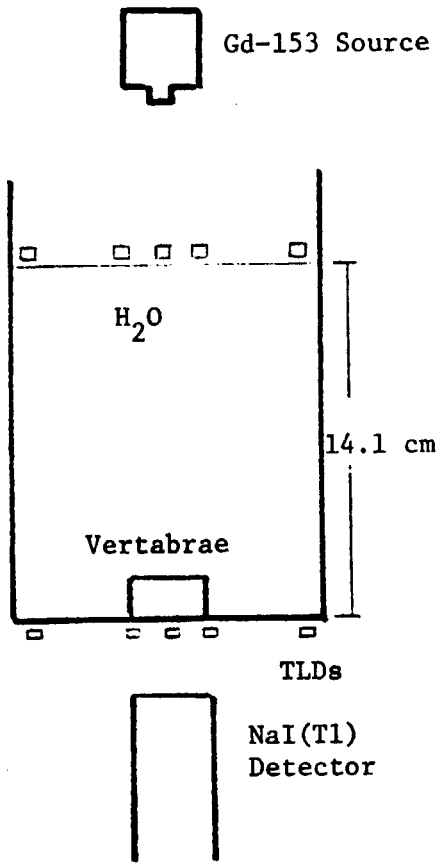

a.) Side View

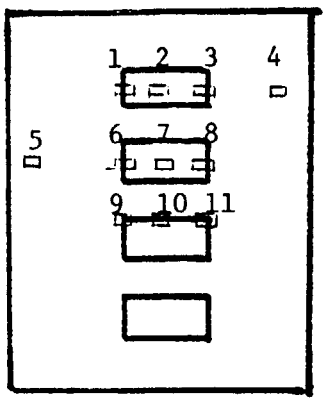

b.) Top View
TLDs on bottom
of tank

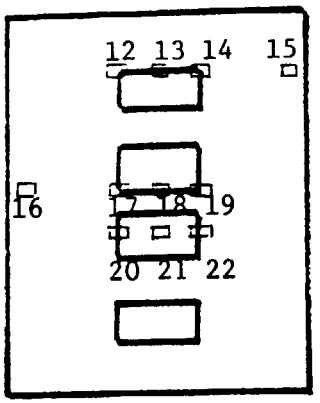

c.) Top View
TLDs on top of tank

Figure 2 Diagram of transmission scan apparatus for determination of radiation dose to the trunk when measuring bone mineral content of the spine.

TABLE 1

Arm Phantom		Spine Phantom	
TLD #	Dose(mrad)	TLD #	Dose(mrad)
1	11.4	1	14
2	35.5	2	14
3	36.2	3	15
4	37.0	4	13
5	35.9	5	15
6	34:0	6	17
7	18.4	7	16
8	21.7	8	16
9	19.3	9	17
10	19.1	10	18
11	16.6	11	17
12	8.5	12	46
		13	51
		14	52
		15	23
		16	24
		17	50
		18	62
		19	58
		20	46
		21	60
		22	55

7. Radiation Sensitivity of the Thyroid During I-131 Therapy

Information on iodine uptake, the effective half-time of its retention in the thyroid and thyroid mass are used in calculating the amount of I-131 to be administered to patients in the treatement of hyperthyroidism. A major variable, however, which we have not yet learned how to assess is radiation sensitivity of the thyroid.

In our work on iodine kinetics, to date, we have evaluated iodine metabolism in large numbers of patients during treatment of thyrotixicosis and have determined model parameters which are reasonable predictors of absorbed radiation dose to the thyroid, given knowledge of thyroid gland size.

Physicians differ greatly in their ability to estimate thyroid gland size by palpation. It is generally agreed that estimates can be off by as much as 100%, although some persons who have devoted significant effort to improve their skills may be within 20% of the true weight, as revealed by analysis of correlations with surgical specimen weights. The use of gland size estimates from outlines of scan defined margins is an imprecise predictor, but does correlate strongly with gland size. The use of x-ray fluorescence provides analogous measurements of gland dimensions based on iodine content distribution, which also correlates very well with gland size (Figures 1 and 2). In addition, given a known iodine content per unit mass of thyroid tissue one could predict thyroid weight with great accuracy in hyperthyroid patients since one can measure iodine content with high precision. However, iodine content/gm is not constant, and needle biopsies are rarely performed in hyperthyroidism and hence this is not a practical answer to the mass estimation problem at this time. The remaining technique which works, in principle, but is not used routinely involves the use of ultrasound, to determine thyroid volume. By multiple passes over the thyroid, cross-sectional maps can be established from which estimates of thyroid volume (and hence mass) can be computed. We had proposed to use this technique in patients going to surgery for thyroid resections and on fresh cadavers prior to autopsy and to evaluate the accuracy of this method. However, attempts at imaging the thyroid with B-mode ultrasound are not yet satisfactory, due in large part, to the quality of the probe available to us. We have continued to use the results of x-ray fluorescence and isotope emission measurements, along with neck palpation, to assess thyroid size for therapy dose calculations.

To evaluate thyroid sensitivity, we need to measure a parameter that refelcts damage to the thyroid. The rate of loss of iodine from the gland following therapy is due to altered rates of release of iodine from the gland and by diminution of uptake. We have measured the iodine content of the gland after therapy, by means of x-ray fluorescence scanning in a large number of patients, in a attempt to determine if predictions of hypothyroidism can be made from the early changes in iodine content after therapy. We are currently measuring iodine content and other thyroid function parmeters in 45 patients who have received radioiodine therapy. These patients have been followed for as long as 14 months post-therapy. These data are shown in Figures 3 - 6. The data are separated in two ways. Figures 3 and 4 show the data grouped in two categories, one with initial iodine content less than 15.5 mg. (1 standard deviation above the normal mean) and the other greater than 15.5 mg. The x at the end of a particular patients' curve indicates that the patient became hypothyroid and was placed on thyroid replacement medication at that time. We currently have six patients in that category. The second grouping is shown in Figures 5 and 6. These figures separate the patients into those who had antithyroid durg medication before and after therapy and those who did not.

Two patients relapsed into hyperthyroidism (shown by the dashed lines in the figures) and received a second therapy dose. We have collected blood samples from most patients throughout their course of study. These samples have been frozen and are being held until the thyroglobulin radioimmunoassay is established. We will then determine thyroglobulin and TSH levels and correlate these with the iodine content data in an attempt to develop a prediction equation which will identify which patients will become hypothyroid, following treatment, on the basis of these data.

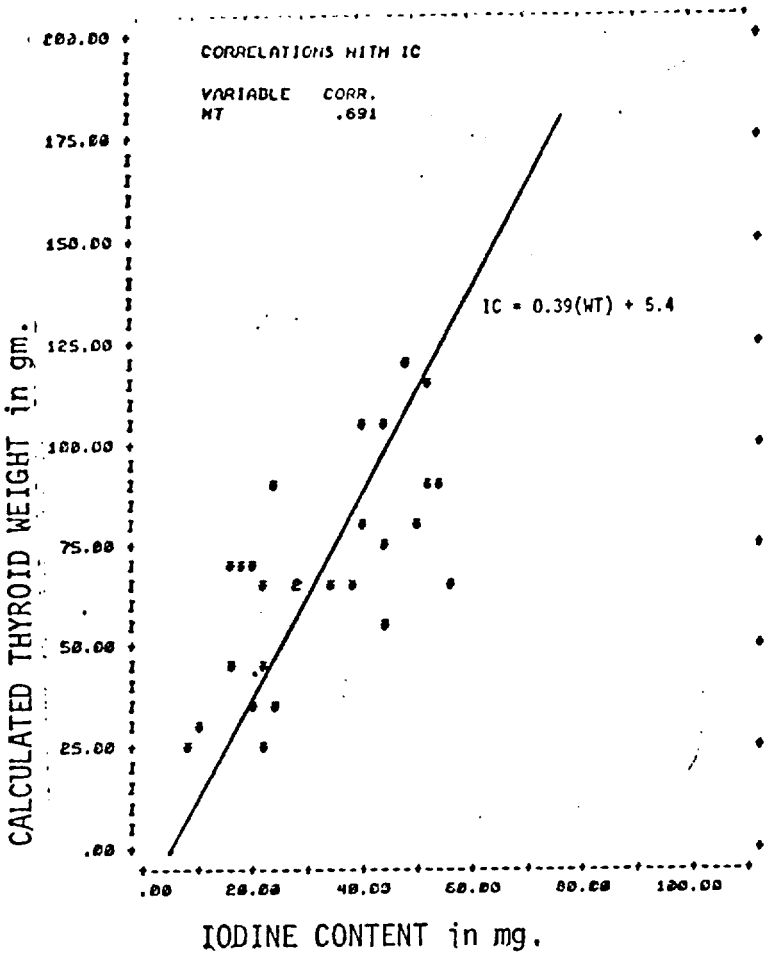

Fig. 1 Plot of estimated thyroid weight vs. iodine content. Values for both variables were obtained from quantitative fluorescent scans of the thyroid.

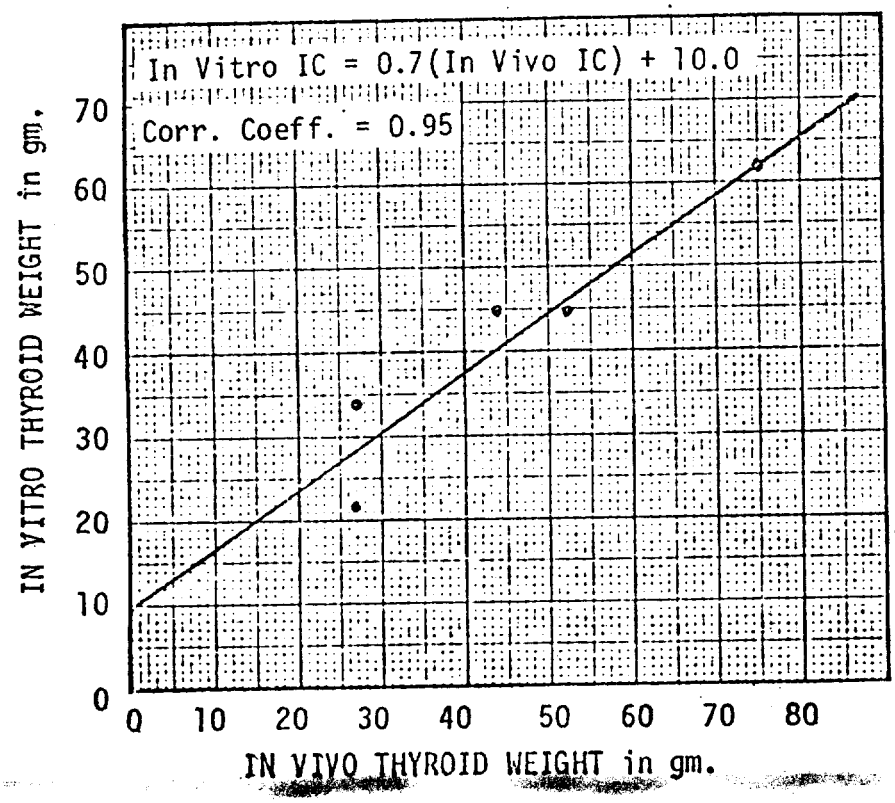

Fig. 2 Plot of in vitro weight as determined post-surgery vs. in vivo weight of the thyroid as determined from quantitative fluorescent scans.

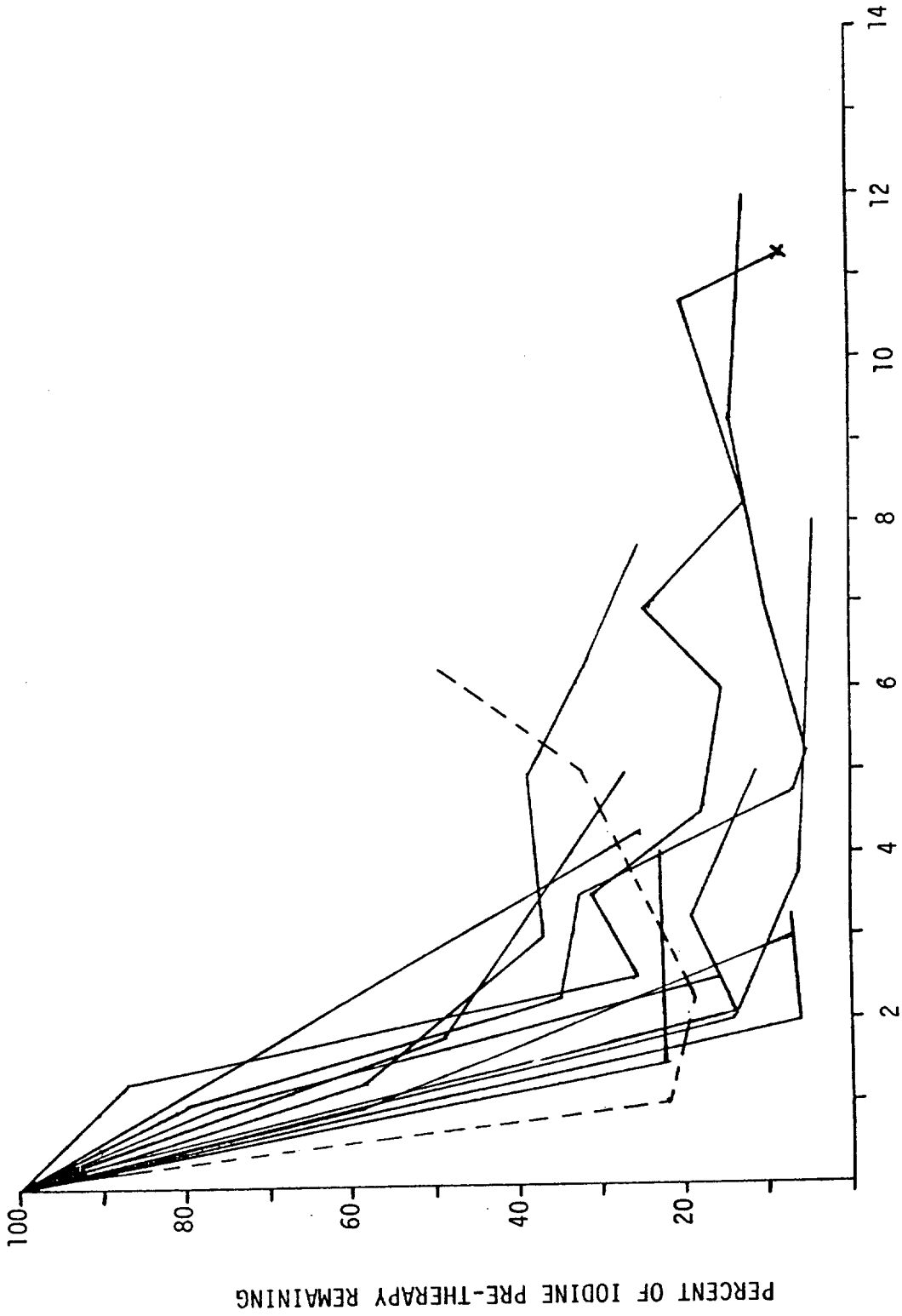
PATIENTS WITH INITIAL IODINE CONTENT LESS THAN 15.5 MG.
PERCENT OF IODINE PRE-THERAPY REMAINING
100
80
60
40
20
2
4
6
8
10
12
14
MONTHS POST-THERAPY

Figure 3

PATIENTS WITH INITIAL IODINE CONTENT GREATER THAN 15.5 MG.

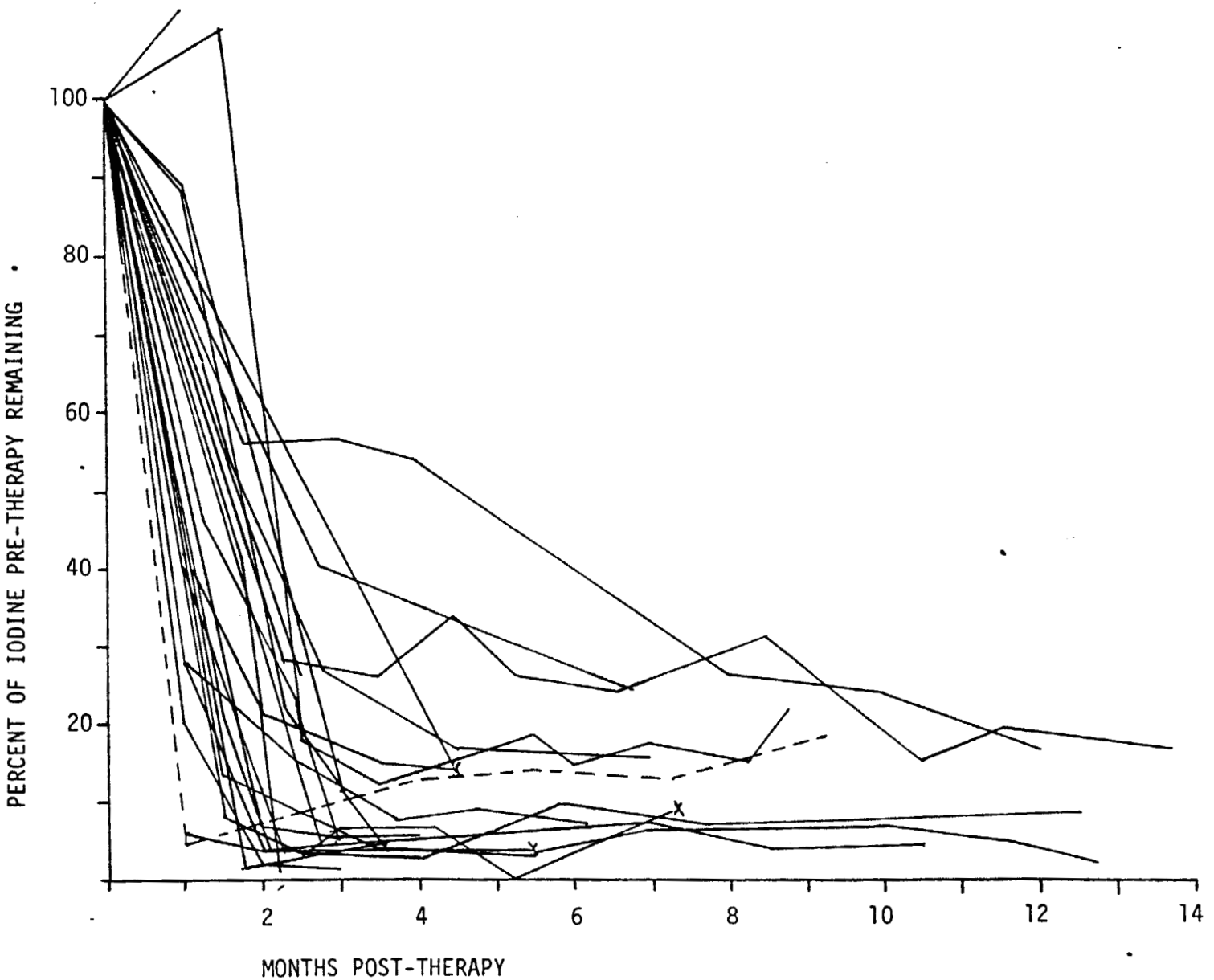

1034754

Figure 4

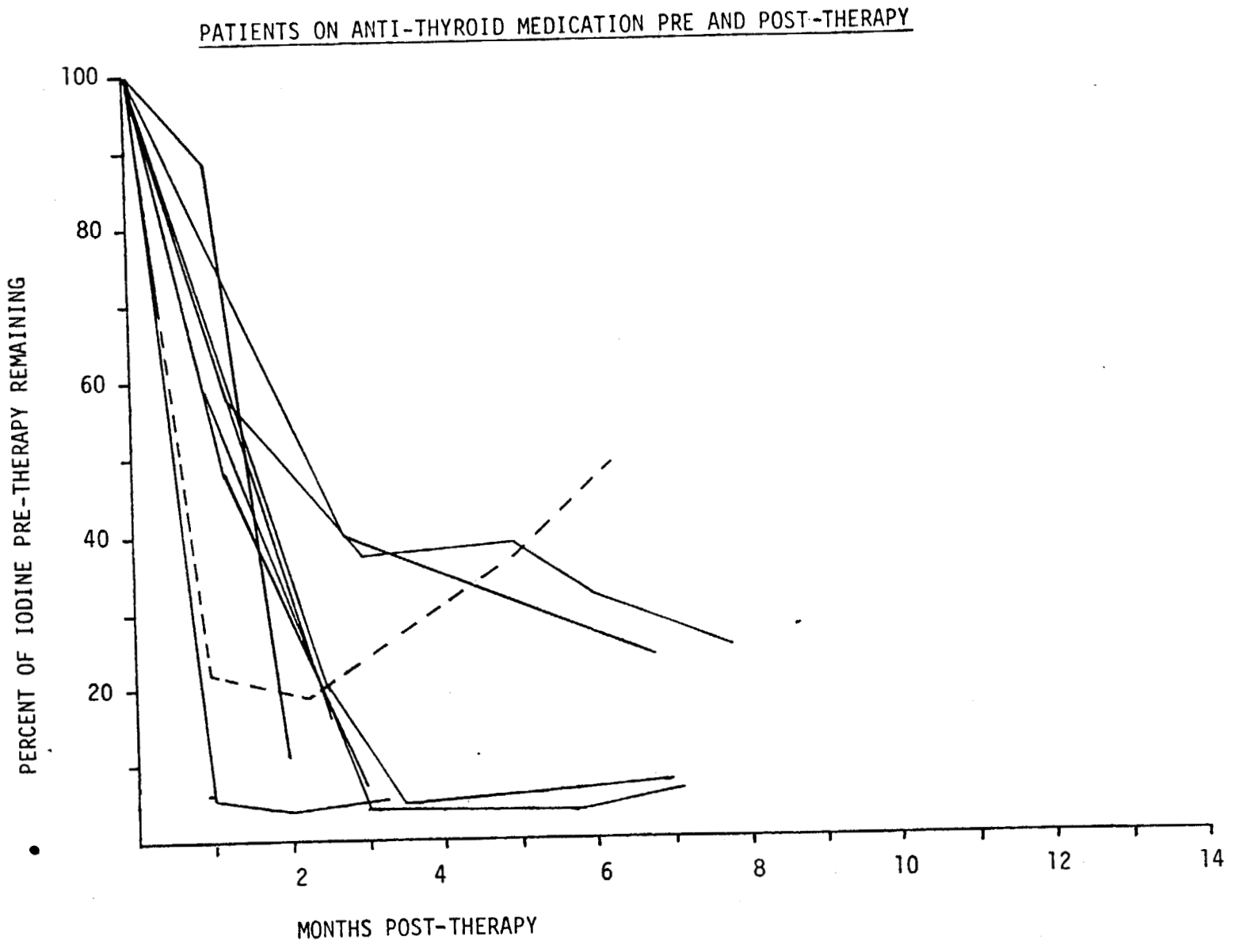

Figure 5

1034755

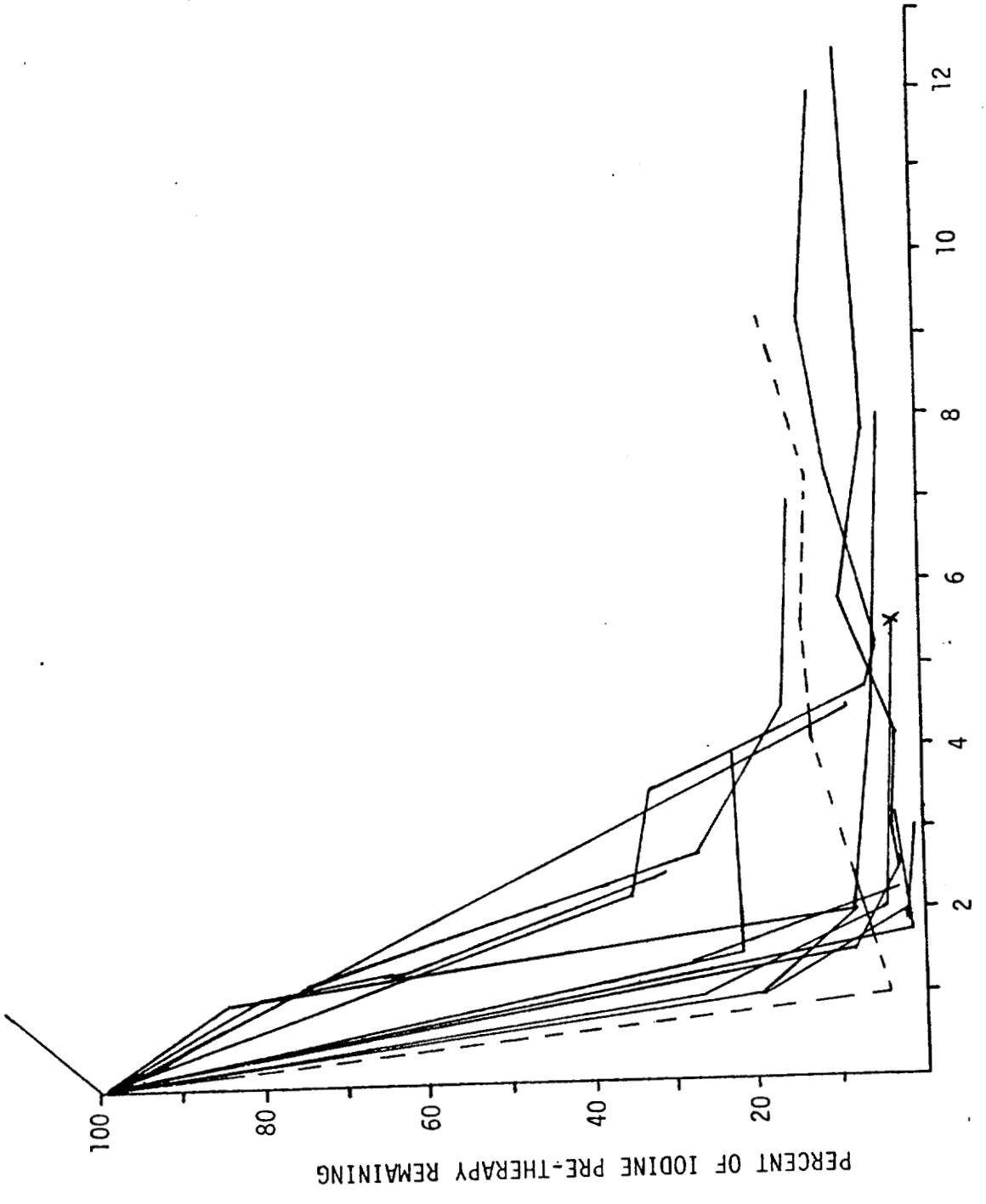

Figure 6

1034756

8. Dosimetry of Myocardial Scanning Agents

Much work is currently being done at Vanderbilt and other laboratories to develop techniques for imaging and delineating areas of myocardial ischemia in patients suspected of suffering from heart disease. The two most common isotopes currently being used are Tc-99m pyrophosphate (Tc PYP) which accumulates in damaged heart muscle and potassium analogs such as Tl, Rb or Cs isotopes which accumulate in normal heart muscle. Simultaneous mapping of the two distributions, (one hot and the other cold), should offer more information than single isotope studies. We planned to explore this possibility in dogs with experimentally induced infarcts. We also planned to obtain dosimetry data from animal studies conducted with suitable isotopes of these elements using the germanium system (i.e. TcPYP, Tl-201, Rb-81, and Cs-131). These radionuclides were selected due to energy and half-life considerations. This system has the spatial resolution necessary to perform these studies in small animals and also has the capability of performing longitudinal section tomography with multiple isotopes simultaneously described in section B.1.b. These studies have been delayed due to space limitations in the department which were resolved July 5, when we obtained an additional 5,000 square feet for clinical imaging studies.

To perform imaging studies on patients with suspected myocardial infarcts, we have interfaced an Ohio Nuclear mobile camera to our computer systems by means of a cable network from the computer room in nuclear medicine to the cardiac intensive care unit, and to the surgical research area. Thus it is now possible to obtain digital data from the scanning agents used in patients and to correlate human studies with those performed in animals.

B. Supporting Systems

1. Hardware Development

B.1.a. CAMAC Autonomous Crate Controller

During the past year we have proceeded with the development of an autonomous CAMAC crate system for remote, stand-alone data collection. To facilitate transmission of data into our PDP/9 system for more comprehensive analysis, we have designed and implemented a direct memory access (DMA) dataway for this machine. This was designed such that it simulates an input/output CAMAC module and is easily used for any number of data collection applications.

We had initially planned to use a prototype INTEL 8080 microprocessor driven autonomous CAMAC crate loaned to us by FNAL. However, the prorotype unit didn't work reliably, and delayed development work on the system until we received a production unit in April 1977.

The system which we are currently using is shown in Figure 1 . In order to gain experience in developing software for the system, i.e. both PDP/9 and 8080 software, we have implemented a configuration which provides us with the ability to digitize video images of clinical X-rays for use in quantitative organ sizing in connection with our ongoing pharmaceutical dosimetry investigations.

The initial implementation of this system involved assembling the 8080 software using a cross assembler (obtained from FNAL) running on the University's Sigma 7 computer. We have since produced our own crossassembler using the Macro-assembler of the PDP/9. In actual use, the CAMAC system is down loaded from the PDP/9 through the RS232 TTY line. This requires approximately 2 minutes for completion.

Once loaded the program is controlled via the console DECwriter of the PDP/9 for region of interest selection and data collection. Once an ROI is selected the area is digitized a column at a time and stored in the 8080 memory. At the end of each column the digital data is transferred in block mode via a CAMAC output register to the DMA port of the PDP/9. Operating in this mode an entire video frame in a 512 x 512 array can be stored in the PDP/9 in 90 seconds. Because of the unexpected delay in delivery of a reliable INTEL 8080 controller the implementation of DMA access to the INTEL 8080 memory as described in the work proposed for 1976-1977, was delayed and is not yet completed.

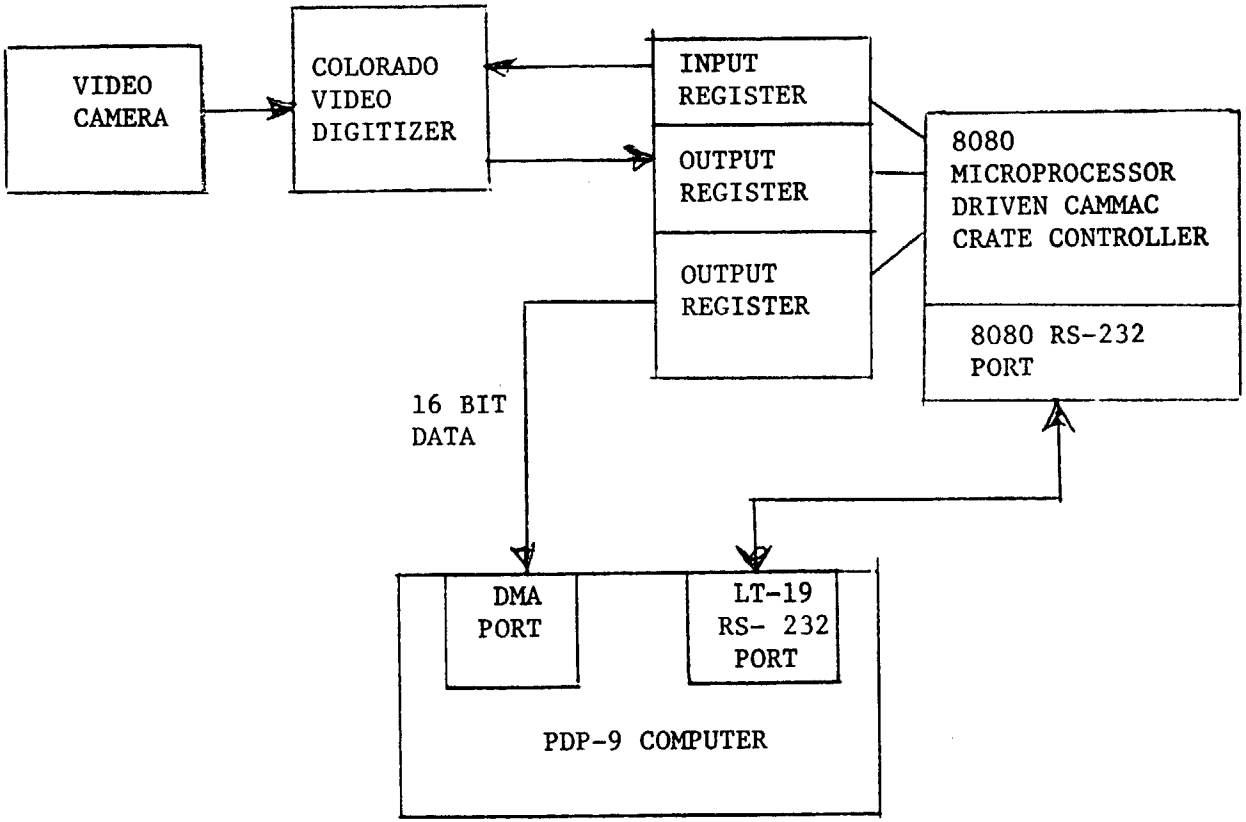

Figure 1. Autonomous CAMMAC crate system used to digitize video images with data being transfered to the PDP-9 through a direct memory access (DMA) port. The program for controlling the 8080 microprocessor is loaded from the PDP-9 through the RS 232 connection.

B.1.b. Intrinsic Germanium Detector Array

The use of solid state or semiconductor detectors makes it possible to map very accurately isotope distributions (good spatial resolution) and permits the simultaneous mapping of multiple isotope distributions (good energy resolution). These two characteristics of semiconductor detectors make them very attractive for use in obtaining internal dosimetry data for radioisotopes. However, low sensitivity due to small size has limited the usefulness of these detectors. To solve this problem, Goulding and Pehl designed and fabricated a mosaic detector system at the Lawrence Berkeley Radiation Laboratory under funding by a one year grant from NIH (April 1974-1975). This system arrived at Vanderbilt in November 1975 and preliminary evaluations and monitoring of the system have been performed.

The intrinsic or high purity (HP) germanium (Ge) detector array shown in Figure 1 consists of 9 detectors each 35mm in diameter, 10mm thick, and arranged in a 3 x 3 matrix with 50mm between centers. The 9 detectors are cooled by a common liquid nitrogen reservoir. The electronics associated with the system include two single channel analyzers (SCA) for each detector coupled to the linear amplifiers. All nine detectors are powered by a common high voltage supply with a voltage divider network employed to maintain each detector at its optimum operating voltage. Energy resolution and relative sensitivity measurements made with a point source of Tc-99m at 1 meter from the front surface of the detectors show that the detectors and electronics are very closely matched and the energy resolutions are excellent (1.06 - 1.18 keV at 140 keV).

For routine frontal plane scanning 19 hole focussed collimators with a geometric resolution of .56cm and a focal length of 8.25 cm have been designed and constructed. These collimators have excellent resolution and relatively uniform response from 2 to 13 cms from the face of the collimator.

The detector electronics have been interfaced to a PDP/11 minicomputer via CAMAC for data acquisition. The system is designed to remain stationary during an imaging procedure with the object to be imaged being moved in an x-y raster. Two modes of operation are available with the instrument.

For phantom and small animal studies the collimated system is suspended over a precision stepping motor-controlled x-y drive system. This scanning system is also interfaced to the PDP/11 computer via CAMAC as shown in the block diagram in Figure 2. The x-y scanner is moved in a rectilinear raster under computer control and data are collected from each of the 18 single channel analyzers (2 for each detector, i.e. 2 photopeaks) simultaneously. Computer programs have been written such that by moving the object to be scanned in a 50 x 50 mm raster (50mm is the distance between detector centers) and collecting 21 x 21 (medium spatial resolution (2.4 mm/point)) or 42 x 42 (high resolution (1.2 mm/point)) data points from each detector a 64 x 64 or 128 x 128 array can be constructed corresponding to a 150 x 150 mm scan field. The detectors and electronics are very closely matched in

efficiency and performance making it possible to normalize between detectors by counting a plane source of activity with each detector and thereby obtaining correction factors.

For large animals and patients the computer is interfaced to our scanning bed (dashed lines in Figure 2) which can be moved in an x-y raster under computer control. This interfacing was accomplished initially on our PDP/9 computer via CAMAC and the same system is being adapted for use with the PDP/11. The system operates in the same fashion as for the stepping motor-controlled system described above. In scanning areas larger than 150 x 150mm, the scanning bed is programmed such that multiple scan fields will be mapped and the resulting data rearranged in the computer to produce a single image corresponding to the total scan field. A C-frame support has been designed and constructed (Figure 1) so that the detector array is suspended over the scanning bed with only possible movement being in the vertical direction for positioning. The detector system is self-contained with the electronics mounted at the back of the C-frame.

Studies have been delayed with this system using the scanning bed due to the unavailability of space in which to operate the system. This space has recently become available so that studies with large animals and patients can be performed in the coming year.

For tomographic applications a second set of collimators has been constructed with the same individual response characteristics as described earlier. However, these collimators are mounted such that their fields of view intersect at a point 6.35cm directly below the central detector as shown in Figure 3. If we define the plane mapped by this common view point as the focal plane of the system, then we can obtain a good representation of the radioisotope distribution in that plane by simply summing the data collected from all detectors. However, images of planes lying above and below the focal plane can also be obtained by maintaining the data separately and recombining after suitable transformations have been performed.

To demonstrate the longitudinal section scanning capability of the system a phantom was scanned consisting of the number 1, 2, and 3 filled with a solution of Tc-99m and positioned at distances of 3, 6, and 9cm from the collimator face in a parafin medium. Tomographic images constructed in the planes of the numbers are shown in Figure 4. The numbers are well resolved by this technique.

Since the system has two energy windows per detector it is also possible to perform simultaneous dual-isotope tomography. This is demonstrated in Figure 5 with tomographic images displayed from a point source of Co-57 (122 keV) positioned 1 cm along the largest void in the Picker thyroid phantom containing a solution of Tc-99m (140 keV). Excellent separation of the distributions is demonstrated. Tomographic images obtained by scanning the 90 and 180 keV photopeaks from the Ga-67 distribution in a rat are shown in Figure 6. The images demonstrate planes of activity with separations of 1.25 cm.

For multiple window studies (i.e. more than two windows per detector) a multiple ADC CAMAC module has been obtained. Electronics have been designed such that analog pulses from the individual detector amplifiers can be digitized and multiple photopeaks separated in the computer. This capability will be extremely useful in performing simultaneous dosimetry studies with multiple isotopes in animals and also in humans.

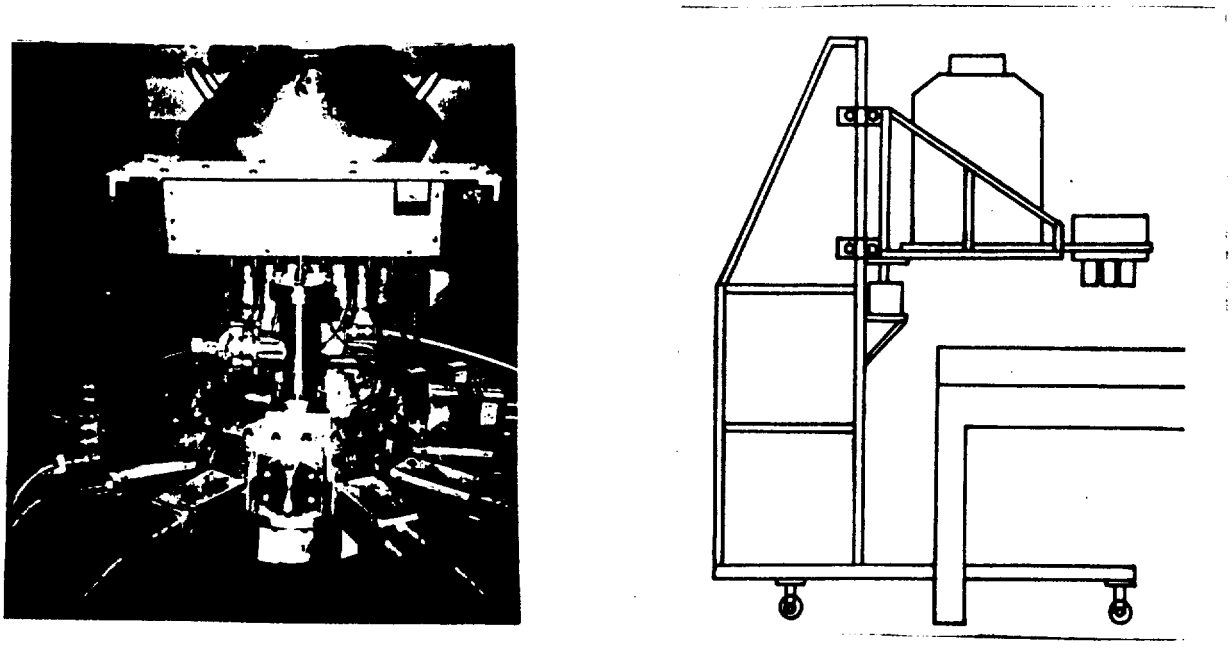

A. B.

Figure 1. (A) Photograph of 9 detector array of high purity germanium detectors. (B) Diagram of frame from which the detector system is suspended over the object to be imaged.

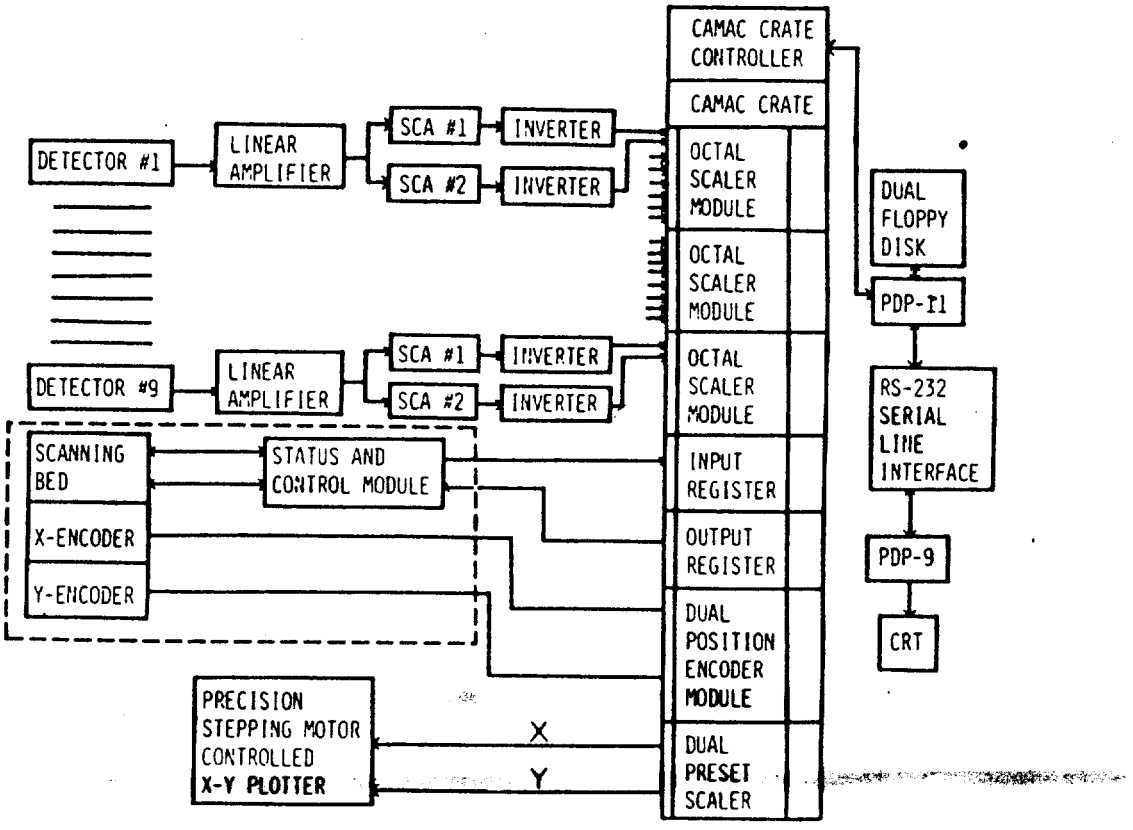

Figure 2. Block diagram of data acquisition system.

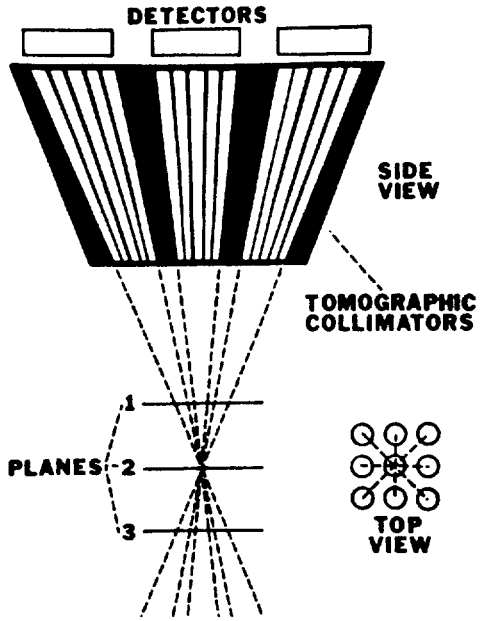

Figure 3. Schematic of the collimator assembly constructed for longitudinal section scanning.

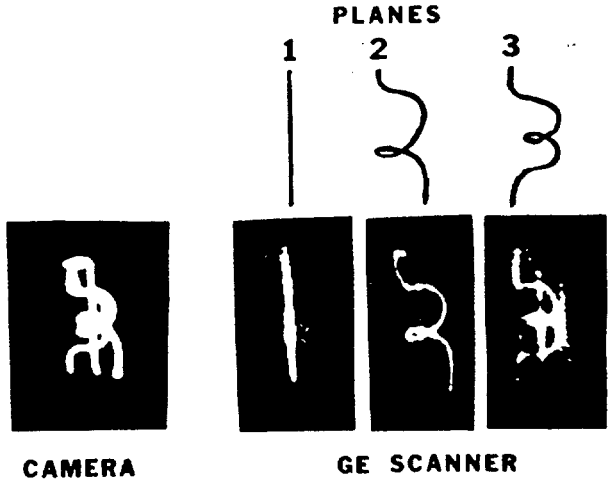

Figure 4. Images of a 3-dimensional number phantom demonstrating the tomographic capability of the germanium system.

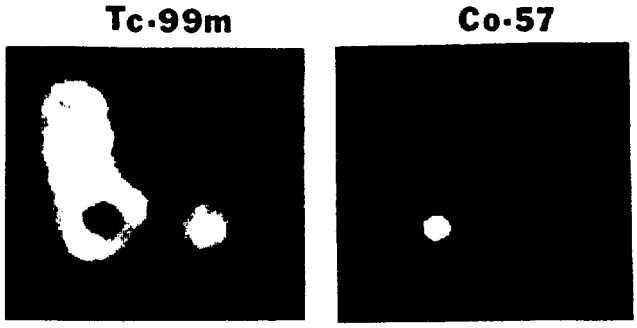

Figure 5. Tomographic images collected simultaneously from the Picker thyroid phantom containing a solution of Tc-99m and a point source of Co-57 placed over the largest void in the phantom.

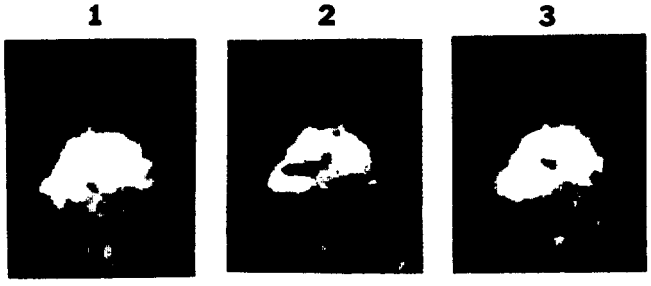

Figure 6. Tomographic images through 3 planes of a rat injected with Ga-67 citrate.

2. Software Development

a. Simulation and Modelling

(i) Specific Dosimetry Projects

We are continuing to develop and test new kinetic models in an effort to understand better the total body and organ retention of these medically administered radioactive materials. Solutions to these models have been sought generally through the use of Berman's SAAM computer program. Our efforts have been directed toward improving model accuracy through the use of external quantitative measurements as supplemental to routine kinetic data. Models are currently being used to analyze data from studies of Fe-50, I-131 Iodocholesterol and iodine kinetics in addition to a number of new radiopharmaceuticals. The details of these models and model calculations have been discussed in the preceeding sections dealing with the specific material.

(ii) SAAM Workshop

During the past year, we organized and co-sponsored a Seminar-Workshop for users of the Simulation, Analysis and Modelling Program (SAAM) developed by Dr. Mones Berman at the NIH. The SAAM program is well known and widely used as a tool for analyzing radiopharmaceutical kinetic data for the purpose of determining organ retention curves and cumulative activities. The SAAM workshop was held this past year at the Oak Ridge Associated Universitites Headquarters building on April 28-31. The other sponsors were the Biomedical Computing Technology Information Center and Dr. Mones Berman's group at the Laboratory of Theoretical Biology, NCI. The meeting covered the current features and uses of the SAAM program and was attended by approximately 40 people from throughout the country. A list of the attendees and a copy of the program have been included as an appendix to our current report.

During the meeting a SAAM users group was created with R. Price being chosen as the coordinator. During the coming years, we are proposing to sponsor seminar--workshops on SAAM and related simulation problems on a regular (hopefully, annual basis). These workshops will serve as a mechanism for people who are working in the area of kinetic modelling to gather, discuss current topics and disseminate new ideas.

b. Sharing of Computer Programs in Nuclear Medicine

During the coming year we plan to intensify our efforts to assist ORNL in the demonstration of the utility of their newly formed information center for the exchange of nuclear medicine software packages. We are working with the personnel of the Biomedical Computing Technology Information Center (BCTIC) in Oak Ridge at several levels. Dr. Brill is a member of the Advisory Committee. Dr. Erickson is co-directing the production of a Nuclear Medicine Computing Directory. This directory of nuclear medicine computers users was first published in July 1976. A copy has been included as an appendix to our current report. At present, it contains descriptions of over 80 U.S. and 20 foreign installations where research is being carried out in the application of computers to nuclear medicine problems. This will greatly facilitate the interchange of software since it describes available computer systems and provides available computer systems and provides software, hardware and clinical contacts at the various institutions. We will continue to submit appropriate software packages to BCTIC for distribution to interested installations. Any new software which we develop--especially in regard to the autonomous CAMAC crate and the various dosimetry studies, will be designed with the intention of their being shared with other interested scientists. In addition, we will continue to assist in identifying available software of relevance to nuclear medicine and will assist

in obtaining its submission to BCTIC and in its subsequent testing prior to distribution.

C. Conferences

i. Vth International Conference on Information Processing in Medical Imaging

Fostered by our continuing interest in quantitative medical imaging, we recently organized and hosted the Fifth International Conference on Information Processing in Medical Imaging (June 23-July 1, 1977). The meeting brought together a large group of internationally recognized experts representing a variety of medical imaging disciplines. These included diagnostic radiography, computerized tomography, ultrasound as well as nuclear medicine. The meeting provided 40 presentations of original work including both invited and offered papers. The meeting format was designed to provide ample time for detailed development of the topics followed by lengthy discussions (1 hour per presentation) in an effort to acheive a maximum in the transfer of information and ideas.

The meeting was highlighted by papers on new quantitative techniques for the construction and display of truly 3-dimensional images and the development of real-time ultrasonography.

The total attendance was approximately 100. A list of the delegates and attendees are included in Appendix VI.

The Sixth Conference in this series is now being organized and will be held in Heidelberg, Germany in 1979.

ii. IEEE Nuclear Medical Science Short Course

The Nuclear Medical Scientist Section of the IEEE Nuclear and Plasma Sciences Society has been in existence for two years. Dr. Brill was the Section Chairman in 1976, and as such was responsible for the organization and conduct of the New Orleans meeting, as well as the Publication of the Proceedings. (IEEE Tr. Nuc. Sci., NS-24, No. 2, April, 1977.) The one day meeting covered 3-D Image Reconstruction, and a Technology Update Session.

The first papers presented described prototypes of the different types of transmission computerized tomography systems that are now available commercially. These included Ohio Nuclear, EMI, Varian, and A. S. & E. systems which were chosen to represent the different classes of instruments currently being marketed. An assessment of the basic physics, problems and potential was presented by Professor Harold Johns.

Four papers were presented on emission tomography, with Gerd Muehllehner giving the introductory discussion. He reviewed the different types of systems used for 3D gamma ray and positron annihilation mapping, followed by presentations of the Massachusetts General Hospital system (Gordon Brownell), the PETT system (Nizar Mullani), ring geometry systems (S. Derenzo) and the Searle Dual positron camera system (G. Muehllehner).

In the technology update session Guy Armentrout summarized data on high-z semi-conductors he had presented in the general session of the IEEE Meeting. Papers on fast scintillators, photo-optical devices, and disk storage systems for video signals were presented and are included in the published proceedings, along with an article on mathematical reconstruction techniques by Cho. Charles Masters described a new DeAnza TV display system with examples from medical imaging applications. The current state of CCDs for image and signal processing was summarized by Robert Hewes of Texas Instrument Corp.

The meeting was attended by approximately 100 people whose active participation suggests that they got something from the exchange of ideas with

other workers in a rapidly moving field in which new technology is playing a major role.

This years program will be arranged by Dr. Glenn Knoll of the University of Michigan. We hope that persons who are involved in developing and using new instrumentation in medicine, particularly in nuclear medicine, will take an active part in future meetings of this section, and will ourselves continue to support this program.